Detailed investigation of doping in hydrogenated amorphous silicon and germanium

M. Stutzmann,* D. K. Biegelsen, and R. A. Street
Xerox Corporation, Palo Alto Research Center, Palo Alto, California 94304
(Received 1 October 1986)

Substitutional doping of hydrogenated amorphous silicon (*a*-Si:H) and germanium (*a*-Ge:H) with phosphorus, arsenic, and boron has been investigated, with use of electron-spin-resonance techniques, optical absorption, and transport measurements. Doping-induced changes in the density of shallow states and deep defects (dangling bonds) are compared for the different doping-host systems. Hyperfine spectra of neutral donor levels are observed in spin resonance and used to deduce a microscopic picture of the underlying donor wave functions. Based on the dependence of the occupancy of deep and shallow states on doping levels and temperature, a detailed model for the electronic density of states in *n*-type *a*-Si:H and *a*-Ge:H below the conduction-band mobility edge is obtained. Furthermore, similar studies in nominally compensated *a*-Si:H are used to discuss the location of boron acceptor states in this material as well as questions concerning light-induced creation of metastable dangling bonds. Experimental evidence for the existence of exchange-coupled electron-hole pairs in compensated *a*-Si:H is presented. For an investigation of the doping process, the incorporation of the various dopant atoms from the deposition gas phase into the amorphous film has been studied by secondary-ion mass spectroscopy. The concentration of electronically active dopants in the deposited film is related to the total concentrations of dopants in the solid or the deposition gas phase for a calculation of the corresponding doping efficiencies. The results are discussed in the context of previous doping models based on the octet rule for chemical valences and of a new model concerning charge-induced structural transitions between weak bonds and dangling bonds.

I. INTRODUCTION

Hydrogenated amorphous silicon, *a*-Si:H, is at present the most extensively studied and also the best understood amorphous semiconductor. The great interest in this material is mainly due to its promising applications for large-area thin-film transistors, solar cells, and a variety of other devices.[1] Two basic discoveries have made possible the use of amorphous silicon as the base material for electronic devices. The first and probably the most important result is that incorporation of hydrogen (or, more recently, fluorine) as a monovalent bond terminator allows one to reduce the large densities of electronically active dangling-bond defects from $\approx 10^{19}$ cm^{-3} in pure *a*-Si to around 10^{15} cm^{-3} in state-of-the-art hydrogenated amorphous silicon. Microscopically this family of defects can be pictured as nonbonding ("dangling") *sp*-hybrid orbitals of Si atoms in different nearest-neighbor environments. In its neutral state, Si_3^0, a dangling-bond orbital is occupied by a single, unpaired valence electron of the corresponding silicon atom. (In the notation employed in the following, the chemical symbol characterizes the atom at which a given electronic state is localized, the lower index denotes the coordination number of this atom, and the upper index gives the net charge of the state. Thus a dangling-bond Si_3^0 corresponds to a neutral, threefold-bonded silicon atom.) Therefore, the Si_3^0 state is paramagnetic and can be detected in an electron-spin-resonance (ESR) experiment, with a characteristic *g* value of 2.0055.[2,3] The neutralization of the dangling-bond defects has been and still is a major requirement for many applications of amorphous silicon, since the Si_3^0 states lie near the middle of the electronic gap of *a*-Si and therefore can very efficiently capture excess electrons or holes introduced by illumination or carrier injection.[4,5]

The second discovery which helped to make amorphous silicon a potential material for device applications was reported by Spear and LeComber in 1975.[6] These authors found that adding phosphine (PH_3) or diborane (B_2H_6) to the silane (SiH_4) gas used for the deposition resulted in large changes of the absolute values and the activation energies of the dark conductivity. The most reasonable explanation for the observed changes is a substitutional doping effect of the group-V P atoms and the group-III B atoms in analogy to what is seen in crystalline silicon. However, in 1975, it was also widely believed that substitutional dopant states in an amorphous semiconductor were improbable, because the flexibility of a disordered network would accommodate the different bonding requirements of group-III and -V atoms without forcing them into a substitutional, fourfold-coordinated site. Thus, before continuing further, it seems appropriate to recall in slightly more detail the concept of substitutional doping in crystalline silicon and likely modifications of this concept in the amorphous counterpart.

Substitutional doping by group-III and -V atoms in a group-IV crystal is a consequence of the topological constraints imposed by the nearest-neighbor atoms on the possible bonding configurations of the substitutional dopant atom. In the case of fourfold coordinated phosphorus, P_4, the local and the long-range bonding symmetry is preserved, i.e., only (rotationally symmetric) σ bonds between *sp*-hybridized orbitals are formed. This allows us not only to increase the number of bonds from three to

four but also, according to Table I, to achieve the bonding configuration with the largest relative bond strength at the given bond length. The cost, however, is the promotional energy $E_{\rm pro}$ necessary to excite the electrons out of the atomic s and p orbitals into the hybridized sp^3 orbitals. As shown in Table II, this energy is roughly equal to the $s \rightarrow p$ transitional energy, $E_p - E_s$, with typical values around 7 eV for the elements of interest here. Thus, relative to the atomic state, the energy of a substitutional phosphorus atom can be written as

$$E_c(\mathrm{P}_4) = E_{\rm pro} - 4E_{\rm B} + E_{\rm AB} \ , \tag{1a}$$

where $E_{\rm B}$ is the bonding energy gained per electron in the σ-bonding states and $E_{\rm AB}$ the energy necessary to put the additional fifth electron into an empty antibonding orbital.

In a similar way, the corresponding energy of a phosphorus atom with threefold coordination is

$$E_c(\mathrm{P}_3) = 3\gamma E_{\rm B} + E_D \ . \tag{1b}$$

Here, the coefficient $\gamma < 1$ describes the reduction in bonding energy caused by the loss of σ symmetry for the bonds in the P_3 configuration. This leads to an admixture of $pp\pi$ character of the P—Si bonds and thereby, according to Table I, to a significant lowering in bond strength. Moreover, the positive distortion energy E_D in Eq. (1b) takes into account that the surrounding Si network will no longer be in the energetic ground state of the ideal crystal, but will contain distorted and even broken "dangling" bonds. Of course, doping occurs in the crystalline case with an efficiency close to 1, so that empirically $E_c(\mathrm{P}_4) < E_c(\mathrm{P}_3)$, i.e., the loss in bonding energy and the additional distortion energy for the case of threefold coordination outweigh the promotional energy necessary for the fourfold-coordinated configuration.

We have chosen the above "tight-binding" picture for the description of doping in crystalline group-IV semiconductors because it can easily be extended to the case of dopant atoms such as P or B incorporated into an amorphous network of Si or Ge atoms. These amorphous phases, a-Si and a-Ge, can be characterized by a conservation of tetrahedral short-range order, but a complete loss of long-range order, i.e., ordering of bonding configurations extending beyond distances of typically 10 Å.[7–9] If we now consider a dopant atom like P in such an amorphous network, two extreme cases can occur. In the simplest case, the local environment of the dopant atom is similar to that in the crystalline phase. Then, according to the discussion above, the lowest-energy configuration of the dopant atom should be the fourfold-coordinated, doping state with an energy

$$E_a(\mathrm{P}_4) \geq E_{\rm pro} - 4E_{\rm B} + E_{\rm AB} = E_c(\mathrm{P}_4) \ , \tag{2a}$$

where we have to allow for small variations in the bonding energy term $E_{\rm B}$ and the antibonding term $E_{\rm AB}$, due to the inherent bonding disorder. A two-dimensional analog is shown in Fig. 1(a).

The other extreme that can occur in the amorphous network is described by an arrangement of the local bonding environment favoring a threefold coordination of the dopant atom as sketched in Fig. 1(b). In this case, the

TABLE I. Relative bond strength for various bonding configurations at a given bond length (Ref. 60). ($i,j=2,3$.)

Bond	Relative strength
$ss\sigma$	1.0
$sp\sigma$	1.1
$pp\sigma$	1.7
$(sp^i)s\sigma$	1.5
$(sp^i)p\sigma$	2.0
$(sp^i)(sp^j)\sigma$	2.5
$pp\pi$	0.5

TABLE II. Atomic Hartree-Fock energies of s and p orbitals (Ref. 60) and sp^3 promotional energies $E_{\rm pro}$ for various elements [$E_{\rm pro} = \frac{1}{4}N(E_s + 3E_p) - 2E_s - (N-2)E_p = (8 - N/4)(E_p - E_s)$], where N denotes number of valence electrons.

Atom	E_s (eV)	E_p(eV)	$E_{\rm pro}$ (eV)
Si	14.8	7.6	7.2
Ge	15.1	7.3	7.8
N	26.2	13.8	9.2
P	19.2	9.5	7.7
As	18.9	9.0	7.5
B	13.5	8.5	6.3
Al	10.7	5.7	6.2

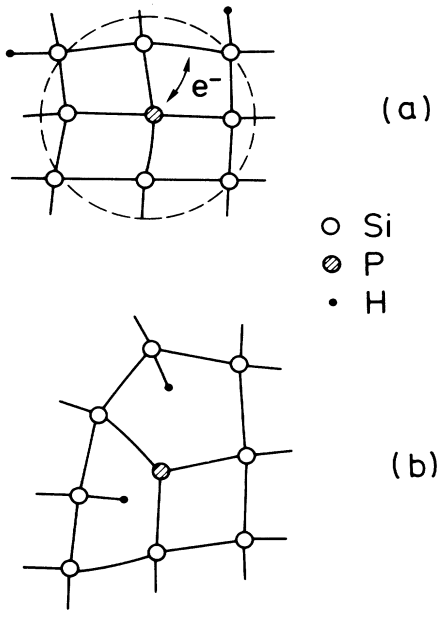

FIG. 1. Schematic models for electronically active (a), and inactive dopant configurations (b) in amorphous silicon or germanium.

phosphorus atom can form strong σ bonds with three network atoms without causing significant additional distortion of the already disordered network. We may thus write approximately

$$E_a(P_3) \approx -3E_B \ . \tag{2b}$$

since according to Table I σ bonds between two sp^3 orbitals or between one sp^3 and one p orbital are of comparable strength.

If we compare Eqs. (2a) and (2b) and note that $E_{pro} > |E_B|$ (approximately 7 eV versus <4 eV) it is clear that in our idealized amorphous network the nondoping, threefold configuration, P_3, is favored energetically. Qualitatively, one can say that the flexibility of the amorphous network allows each atom to achieve the same bonding coordination as it would in an unconstrained, molecular state (e.g., silicon and germanium fourfold coordinated as in SiH_4 an GeH_4, and phosphorus threefold coordinated as in PH_3), whereas the structural constraints exerted by a crystalline environment impose on the dopant atoms the bonding symmetry of the host network. These arguments underly Mott's 8-N rule.[10]

It came, therefore, as a surprise when substitutional doping was discovered in hydrogenated amorphous silicon and germanium, and a large number of investigations have been performed in order to explain and to exploit this phenomenon. Most of the work has centered on phosphorus- and boron-doped a-Si:H, with the application of this material in mind. Many fewer investigations have dealt with doped a-Ge:H, compensated material, or other dopants such as arsenic or gallium. From the physical point of view, to derive a general picture of the doping mechanism in tetrahedrally bonded amorphous semiconductors, comparable experiments performed on a large number of different dopant-host systems would be highly desirable. The purpose of this article is, therefore, to provide a consistent set of data for the most common dopants (P,B,As) in both, a-Si:H and a-Ge:H, using a number of different experimental techniques.

We begin in Sec. II with a detailed description of our experimental results concerning the nature of donor and acceptor states in a-Si:H and a-Ge:H and the quantitative dependence of these states and of other doping-induced defect states (dangling bonds) on the doping level. These data are then used to construct and compare models for the doping dependence of the density of states in both amorphous host materials. In Sec. III doping effects in compensated a-Si:H are discussed. Finally, Sec. IV examines the dopant incorporation during deposition and the doping efficiency for all dopant-host systems, and the consequences of the experimental results for possible doping mechanisms.

II. THE INFLUENCE OF DOPING ON THE ELECTRONIC DENSITY OF STATES

A. Experimental details

The samples used in this study were deposited by rf glow discharge in capacitively coupled reactors. Doped a-Si:H samples were produced at Xerox Palo Alto Research Center by decomposition of undiluted SiH_4 mixed with PH_3, AsH_3, and B_2H_6 under standard conditions (substrate temperature 230 °C, power density 30 mW/cm^2). The substrate materials were aluminum foil and Corning 7059 glass. Doped a-Ge:H was deposited at the University of Marburg under comparable conditions (220 °C, 50 mW/cm^2), using GeH_4 premixed with PH_3 or B_2H_6 and diluted in Ar (volume ratio 1:1). Here, molybdenum and quartz were the substrate materials. Some doped a-Si:H samples were also deposited in this system for cross-checking. The doping profiles of selected samples were determined by secondary-ion mass spectrometry. Gradients of the dopant concentration were negligible in all cases.

Samples used for the magnetic resonance experiments were removed from the aluminum or molybdenum substrates and collected in narrow quartz tubes. The typical volume of a-Si:H and a-Ge:H thus collected was 10^{-2} cm^3, allowing the detection of spin densities $>10^{14}$ cm^{-3} in a-Si:H and $>10^{15}$ cm^{-3} in a-Ge:H. Magnetic resonance measurements were performed using commercial ESR spectrometers (X-band, Bruker ER 200D and Varian E201) equipped with helium-gas-flow cryostats and optically accessible TE_{102} cavities. Defocused monochromatic laser light (647.1 nm) was used in the light-induced ESR (LESR) and the optically detected magnetic resonance (ODMR) experiments. We estimate the absolute error in the spin densities quoted in the following to be about 50%, with a much smaller relative error for the comparison of different samples measured in the same spectrometer ($<10\%$).

Apart from ESR or LESR measurements, the densities of shallow and deep states were also determined (independent of their spin state) by charge sweep-out and optical absorption [photothermal deflection spectroscopy (PDS)] experiments. Details concerning the two latter techniques have been published elsewhere[11,12] and will not be repeated here. It is worth noticing that the absolute densities measured by ESR on one side and charge sweep out and charge counting on the other side always agreed to within the 50% absolute error estimated above.

B. Fermi-level shift and occupancy of intrinsic electronic states

The most direct evidence for the occurrence of doping in a semiconductor is usually the shift of the Fermi level, E_F. Since the discovery of doping in a-Si:H and a-Ge:H, much work has been devoted to document, analyze, and finally, model the doping-induced changes of the transport properties in terms of densities of states, carrier mobilities, etc. For a rather incomplete selection of articles dealing with these problems see Refs. 13–19 and references therein.

The dependence of the dark-conductivity activation energy, E_σ, on the doping level is shown in the lower portion of Figs. 2(a) and 2(b) for the a-Si:H and a-Ge:H samples used in this study, or at least for samples deposited under identical conditions in the same reactor. The doping level is measured in terms of the dopant-gas volume concentration in the plasma. To a first-order approxima-

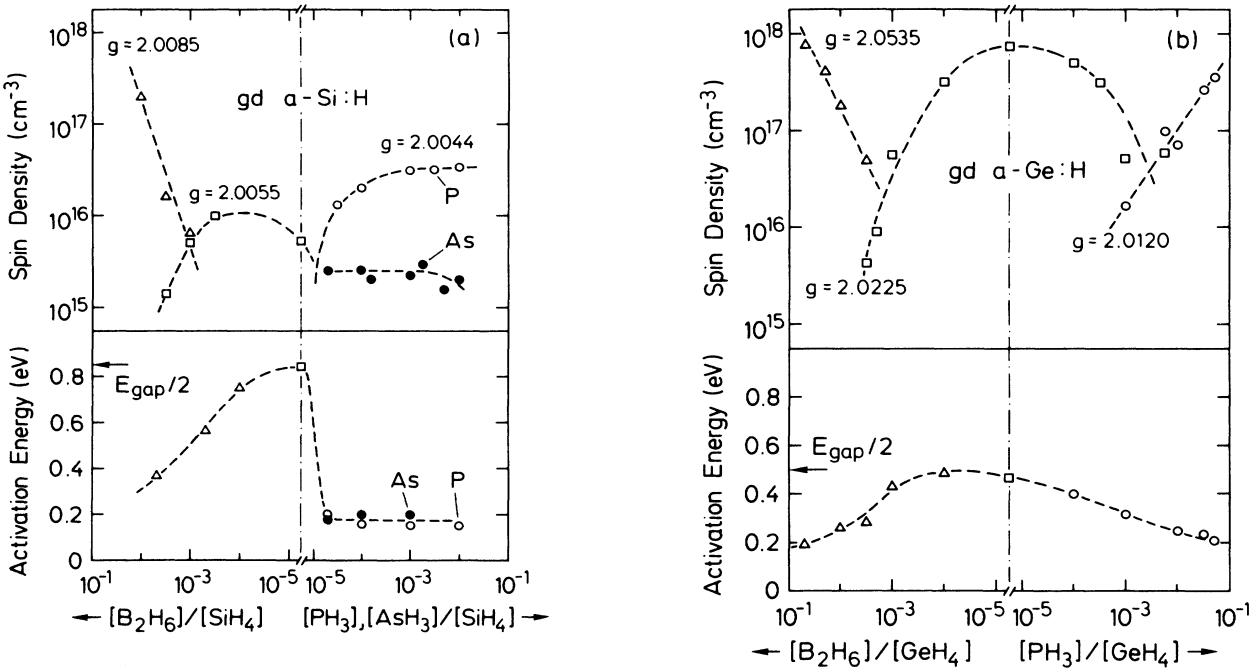

FIG. 2. Electron-spin-resonance defect densities (upper half) and dark conductivity activation energies (lower half) in hydrogenated amorphous silicon (a) and germanium (b) as a function of dopant-gas concentrations. The indicated g values refer to the various defects discussed in the text. Arrows denote the Fermi-level position in the center of the mobility gap. Open and solid circles in (a) refer to phosphorus and arsenic donors, respectively.

tion, the dark-conductivity activation energy is given by

$$E_\sigma^n \approx E_C(0) - E_F(0) + T\frac{d}{dT}[E_c(T) - E_F(T)] \quad (3)$$

for n-type samples with an equivalent expression for p-type material. Here, E_C refers to the conduction-band mobility edge, and T is the absolute temperature. Experimentally, the temperature shifts of the various energies in Eq. (3) are of the order of 10^{-4} eV K^{-1}, so that for typical experimental situations, E_σ^n and E_σ^p are equal to $E_C(0) - E_F(0)$ and $E_F(0) - E_V(0)$ with an accuracy of about 0.1 eV. Therefore, from the data in Figs. 2(a) and 2(b), it can be seen that for both, a-Si:H and a-Ge:H, E_F lies close to midgap in the undoped case (slightly above midgap in a-Ge:H). Upon doping with either boron, phosphorus, or arsenic, E_F moves more or less rapidly towards E_V or E_C. For the highest doping levels, a value of $|E_F - E_{C,V}| \approx 0.2$ eV is reached asymptotically for all dopant-host systems.

The doping-induced shift of the Fermi-level position through the mobility gap of a-Si:H and a-Ge:H can also be observed by ESR. The occupation of the localized gap states depends on E_F, T, and the electron correlation energy, U_{eff}. Generally, U_{eff} can be written as the sum of two terms,

$$U_{\text{eff}} = U_C - U_R \ , \quad (4)$$

where U_C (>0) describes the repulsive Coulomb interaction between two electrons occupying the same localized state, and U_R accounts for the structural relaxation caused by the presence of this second electronic charge in the vicinity of its center of localization. Obviously, the magnitude of U_{eff} will depend on the degree of localization of a given electronic state. Correlation effects will be quite small for a pair of electrons with wave functions extending over macroscopic distances. If $|U_{\text{eff}}| \ll kT$, the occupancy of an electron system will be given to a good approximation by the Fermi distribution, with states below E_F occupied by two electrons, states above E_F empty, and singly occupied states existing only in a region of width approximately equal to kT around E_F. On the other hand, if an electronic state is sufficiently localized, both U_C and U_R can take values significantly larger than kT. In such a case, the occupancy of electronic states near E_F is no longer described accurately by simple Fermi statistics. The two extreme cases which can occur are a large positive correlation energy, $U_C > U_R \gg kT$, and a large negative correlation energy, $U_R > U_C \gg kT$. In the latter case, the electronic system can gain energy by pairing of spins in thermal equilibrium. States near E_F will either be doubly occupied or empty with no unpaired spins and consequently no ESR signals, at least at sufficiently low temperatures. More interesting for ESR investigations is the case of a large positive correlation energy. Then the Coulomb repulsion U_C is large enough to prevent double occupancy of states in an energy "window" of width U_{eff} below E_F. Therefore, a large and temperature-independent density of paramagnetic states can exist and be detected by ESR.

The magnitude and the sign of the correlation energy are important and, unfortunately, still controversial issues of electronic states in the mobility gap of amorphous semiconductors,[20–26] and the same is true for *a*-Si:H and *a*-Ge:H. However, in these two materials, there is increasing experimental evidence for a positive correlation energy, with values $U_{\text{eff}} \approx +0.3$ eV and $U_{\text{eff}} \approx +0.1$ eV for dangling bonds in *a*-Si:H and *a*-Ge:H, respectively, and correlation energies between 10 and 200 meV for the various band tail states.[27–36]

For completeness it should be mentioned that, contrary to these experimental results, a negative correlation energy has also been proposed.[37,38] It is the belief of the present authors, however, that the accumulated experimental evidence is strongly in favor of a positive correlation energy for the large majority if not for all of the states in the mobility gap of *a*-Si:H and *a*-Ge:H. Generally, a very good qualitative and quantitative agreement is observed between measurements of the electronic density of states carried out with techniques which are independent of the spin state (field effect, space-charge-limited current, charge sweep out, deep-level transient spectroscopy, optical absorption) and the various spin resonance techniques, which only can be applied to states with unpaired spins.

In Figs. 2(a) and 2(b), the ESR spin density measured for the various paramagnetic states "intrinsic" to *a*-Si:H and *a*-Ge:H is shown as a function of the gas-phase doping level for the dopant gases B_2H_6, PH_3, and AsH_3. Three types of paramagnetic states are known to exist and can be distinguished by virtue of their energy range and electronic *g* value.[27,28,39,40] When the Fermi level is close to the valence-band mobility edge as in boron-doped samples, a resonance with $g = 2.008 - 2.013$ ($g = 2.0535$ in *a*-Ge:H) is observed. This resonance is ascribed to singly occupied bonding orbitals of the weak Si—Si (Ge—Ge) bonds constituting the valence-band tail. According to Fig. 2, this resonance can be observed for gas-phase doping levels above 10^{-3} in both *a*-Si:H and *a*-Ge:H, where $E_F - E_V$ lies between 0.5 and 0.2 eV. (Note the quantitative agreement between the spin densities of this resonance measured in *a*-Si:H and *a*-Ge:H as a function of Fermi-level position relative to E_V.) In *n*-type material, the corresponding ESR signal of singly occupied weak antibonding orbitals can be seen with $g = 2.0044$ in *a*-Si:H and $g = 2.0120$ in *a*-Ge:H for $E_C - E_F$ in the range 0.3—0.15 eV. Here, quite significant differences in spin density exist between *a*-Si:H and *a*-Ge:H and, notably, between phosphorus and arsenic-doped *a*-Si:H. Finally, in undoped or weakly doped samples, the dominant ESR signal comes from Si or Ge dangling bonds (Si_3^0, $g = 2.0055$; and Ge_3^0, $g = 2.0225$). These different paramagnetic states are intrinsic to *a*-Ge:H or *a*-Si:H, and are distinguished from the dopant states which will be discussed in the next section. The intrinsic nature of the dangling bond and tail states follows directly from the possibility to observe their corresponding resonances in undoped samples by a suitable shift of the quasi-Fermi levels instead of the Fermi level, e.g., by ESR measurements under illumination at low temperatures [light-induced electron-spin resonance (LESR)].[41,42]

The ESR spin-density data and the experimental values for the Fermi-level position as a function of doping in Figs. 2(a) and 2(b) can be combined to obtain an estimate for the electronic density of states, $D(E)$ in the mobility gap of *a*-Si:H and *a*-Ge:H. Specifically, the ESR dangling-bond density of undoped material divided by the effective correlation energy can be used for a calculation of $D(E)$ near midgap. With $U_{\text{eff}}(\text{DB}) \approx 0.3$ eV in *a*-Si:H (0.1 eV in *a*-Ge:H) the ESR data yield $D(E) \approx 10^{16}$ $\text{cm}^{-3}\text{eV}^{-1}$ for state-of-the-art *a*-Si:H, and $D(E) \approx 10^{19}$ cm^{-3} eV^{-1} for *a*-Ge:H. These values compare very favorably to estimates obtained from spin-independent techniques.[43–45] As far as the tail states are concerned, the ESR data can be used to calculate both, the characteristic slope and the integrated charge density of the tails. The band tail slopes follow from the dependence of the ESR spin density in doped samples on the Fermi-level position: $N_S \propto \exp(-\gamma \Delta E)$ with $\Delta E = |E_F - E_{C,V}|$. Experimental values for the slope parameter γ are ≈ 35 eV^{-1} in the conduction-band tail and $\gamma \approx 20$ eV^{-1} in the valence-band tail. Again, both values are in good agreement with other techniques (Ref. 31 and references therein, and Ref. 46). Finally, the ESR spin density observed in heavily doped samples is also an accurate measure of the total integral density of charges localized in the shallow states of the band tails. This is due to the fact that the effective correlation energy of the tail states is positive and has a magnitude comparable to the inverse of the tail-state decay parameter, $1/\gamma$.[31] Hence, the window of paramagnetic states contributing to the ESR signal, which extends from E_F to $E_F - U_{\text{eff}}$, encloses the majority of holes (electrons) localized in the valence- (conduction-) band states. The density of holes or electrons in the band tails can be measured very accurately and in an independent manner by a charge-counting technique which is unaffected by the spin state of the collected charges.[36] The observed charge densities usually agree with the ESR spin densities to within a factor of 2 or smaller for all samples. This good correlation between the electron-spin resonance and the charge sweep-out data in *a*-Si:H doped with phosphorus, arsenic, and boron is demonstrated in Fig. 3.

We end this section by briefly pointing out some qualitative and quantitative differences between the different dopant-host systems in Fig. 2 which will be of importance in the following. First, looking at Fig. 2(a), it is evident that there are large differences between *p*- and *n*-type doping of *a*-Si:H. In boron-doped *a*-Si:H the Fermi level moves only very slowly and continuously from midgap to $E_F - E_V \approx 0.3$ eV. This is consistent with the observation of the ESR dangling-bond signal over a large doping range (up to a diborane concentrations of 10^{-3}), and with the rather slow exponential increase of the valence-band-tail signal at higher doping levels. In contrast, *n*-type *a*-Si:H shows a very rapid jump of E_F from midgap to $E_C - E_F \approx 0.2$ eV with increasing doping level. This asymmetry of the Fermi-level position as a function of doping for *p*- or *n*-type *a*-Si:H indicates either a difference in the doping efficiency for the donors or acceptors employed, or a corresponding asymmetry in the electronic density of states, caused by the larger slope of the conduction-band tail.[47] Moreover, Fig. 2(a) shows that

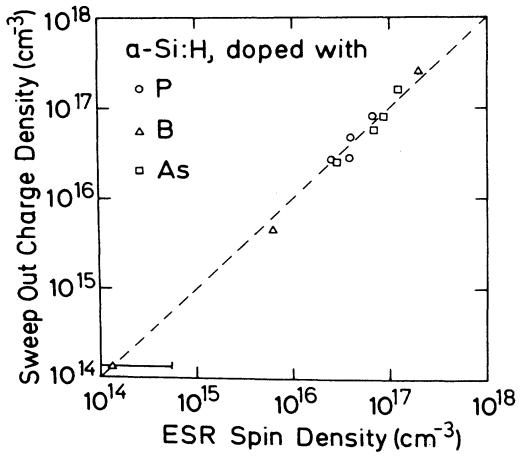

FIG. 3. Correlation between the density of shallow defects as measured by electron-spin-resonance and voltage-pulse sweep-out experiments for P^-, As^-, and B-doped *a*-Si:H.

the density of conduction-band-tail states measured in *n*-type *a*-Si:H is by about an order of magnitude larger in phosphorus-doped material than in arsenic-doped *a*-Si:H. This observation can be explained quantitatively by the different position of the Fermi level in arsenic- and phosphorus-doped *a*-Si:H. In heavily phosphorus-doped amorphous silicon, the Fermi level lies at about 150 meV below E_C, whereas in arsenic-doped samples, $E_C - E_F$ reaches about 200 meV for corresponding doping levels. With a slope of the conduction-band tail of $\gamma \approx 35$ eV^{-1} as quoted above, this 50-meV difference in the Fermi-level position for strong arsenic and phosphorus doping should be equivalent to a change in singly occupied conduction-band-tail states by at least a factor of exp [(35 eV^{-1})/(0.05 eV)] ≈ 6, in accordance with the data in Fig. 2(a). In both, arsenic- or phosphorus-doped *a*-Si:H, the Fermi level remains constant relative to the conduction-band mobility edge for doping levels above 10^{-4}, resulting also in a constant density of conduction-band tail states observed in electron-spin resonance.

A comparison between doped *a*-Si:H and *a*-Ge:H shows that, first of all, the density of dangling bonds in the latter material is usually by about 2 orders of magnitude higher. One consequence of this increased density of states near midgap is that in *a*-Ge:H it takes relatively high doping levels of about 10^{-3} for both boron or phosphorus to shift the Fermi level out of the dangling-bond band into one of the band tails. Above this doping level, *p*-type *a*-Si:H and *a*-Ge:H exhibit a surprisingly similar doping behavior. For example, the doping dependence of the dark-conductivity activation energy relative to the total band gap, E_σ/E_g, is nearly identical for both materials as a function of boron doping, decreasing roughly linearly from a value of ≈ 0.5 for undoped samples to $E_\sigma/E_g \approx 0.2$ for a boron gas-phase doping level of 10^{-2}. This indicates that the electronic density of states in the lower half of the mobility gap is actually quite similar for both materials, except for the mentioned differences of the dangling-bond density near midgap. On the other hand, quite large differences are observed between the transport or spin resonance properties of phosphorus-doped *a*-Ge:H and *a*-Si:H. This is a consequence of the fact that in *a*-Si:H the Fermi level jumps rather abruptly from a midgap position to a position $E_C - E_F \approx 150$ meV upon doping with phosphorus, whereas the same movement of the Fermi level occurs much more slowly in *n*-type *a*-Ge:H. To be more precise, in *a*-Ge:H, again, a doping level of 10^{-3} is needed to achieve a double occupation of the large dangling-bond density of states and to shift the Fermi level into the conduction-band tail. In *a*-Si:H, on the other hand, the pronounced drop of E_σ from approximately 0.8 to 0.2 eV for doping levels as low as 10^{-6} suggests that the electronic density of states in the upper half of the mobility gap in this material is quite low compared to the dangling-bond density of states of about 10^{16}–10^{17} cm^{-3}eV^{-1}. Thus, the electron-spin-resonance measurements reproduce the minimum in the density of states in the upper half of the *a*-Si:H mobility gap, which has also been observed by deep-level transient spectroscopy experiments.[47]

To summarize this section, we show in Fig. 4 the electronic density of states of undoped *a*-Si:H and *a*-Ge:H as it can be deduced from electron-spin-resonance experiments.

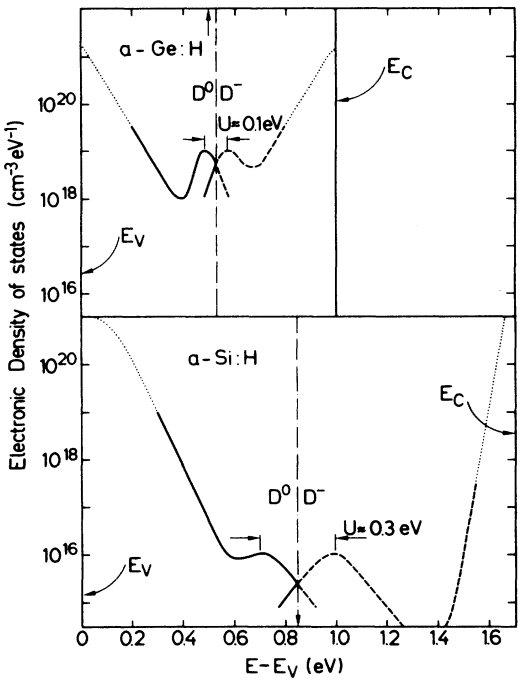

FIG. 4. Models for the electronic density of state in undoped amorphous germanium (upper half) and silicon (lower half) deduced from the combined ESR and transport measurements. Arrows indicate the center of the mobility gap, dashed-dotted lines the Fermi-level position in nominally undoped samples. E_C and E_V refer to the conduction- and valence-band mobility edges, respectively. D^0, D^-, and U denote the neutral and doubly occupied dangling-bond levels and their effective electronic correlation energy.

C. The nature of donor and acceptor states in *a*-Si:H and *a*-Ge:H

1. Donor states

The donor states (P_4,As_4) in *a*-Si:H and *a*-Ge:H are introduced by doping with phosphine and arsine. Unlike in the crystalline materials, the large density of intrinsic tail states in amorphous semiconductors renders the direct observation of the shallow donor states via spectroscopy of their energy levels in the gap very difficult, if not impossible. Again, spin resonance techniques turn out to be very useful, since the spin properties of electrons in intrinsic tail states (CB,VB) are very different from those of the donor electrons. This difference is due to the fact that both donors have a nonzero nuclear spin $I \neq 0$ occurring with an isotopic abundance of 100% (see Table III). As a consequence, electronic spins localized near a donor atom will experience different magnetic environments, corresponding to the various possible orientations of the donor nuclear spin with respect to the electronic spin. In the presence of the additional external magnetic field $\mathbf{H}$ imposed by the ESR experiment, the Hamiltonian of the interacting nuclear and electronic spins can be written as

$$H=\mu_B \mathbf{H}\cdot[\mathbf{g}_e]\cdot\mathbf{S}+\mu_n \mathbf{H}\cdot[\mathbf{g}_n]\cdot\mathbf{I}+\mathbf{S}\cdot[\mathbf{A}]\cdot\mathbf{I} \; . \tag{5}$$

Here, μ_B and μ_n are the Bohr and the nuclear magneton, $[\mathbf{g}_e]$ and $[\mathbf{g}_n]$ the electronic and nuclear $\mathbf{g}$ tensors, and $[\mathbf{A}]$ is the hyperfine coupling tensor. Since we are only concerned with ESR transitions in the following, we can drop the second term, which only contains the nuclear spin, $\mathbf{I}$. Moreover, we will assume that the electronic donor wave function, $\Psi_e(\mathbf{r})$, can be approximated by a spherically symmetric *s*-like function

$$\Psi_e(r)=(\pi a^3)^{-1/2}\exp\left[\frac{-r}{a}\right] . \tag{6}$$

A similar form is also a first approximation for the envelope of the donor ground states in crystalline silicon and germanium.[48] Then, Eq. (5) may be simplified to

TABLE III. Nuclear magnetic properties of various isotopes present in *a*-Si:H and *a*-Ge:H with significant concentrations.

Isotope	Spin I (units of $\hbar$)	Moment (units of μ_n)	Abundance (%)
^{1}H	$\frac{1}{2}$	2.793	100
^{10}B	3	1.801	19.6
^{11}B	$\frac{3}{2}$	2.688	80.4
^{13}C	$\frac{1}{2}$	0.702	1.1
^{14}N	1	0.403	99.6
^{15}N	$\frac{1}{2}$	−0.283	0.4
^{29}Si	$\frac{1}{2}$	−0.555	4.7
^{31}P	$\frac{1}{2}$	1.137	100
^{73}Ge	$\frac{9}{2}$	−0.877	7.8
^{75}As	$\frac{3}{2}$	1.435	100

$$H=\mu_B g_e \mathbf{H}\cdot\mathbf{S}+A\mathbf{S}\cdot\mathbf{I} \; , \tag{5'}$$

where the isotropic hyperfine interaction A is now of the Fermi contact form:[49]

$$A=\left[\frac{8\pi}{3}\right] g_e g_n \mu_B \mu_n \, |\, \Psi_e(0) \,|^2 \; . \tag{7}$$

With $\mathbf{H}=H\mathbf{e}_z$, $\mathbf{S}_{\pm}=\mathbf{S}_x \pm i\mathbf{S}_y$ (similar for $\mathbf{I}_{\pm}$), the spin Hamiltonian (5a) can be written as

$$\begin{aligned} H&=(\mu_B g_e H S_z + A I_z S_z)+[\tfrac{1}{2}A(I_+ S_- + I_- S_+)] \\ &=H_1+H_2 \; . \end{aligned} \tag{5''}$$

The corresponding energy levels $E(m_S,m_I)$ are a function of the electronic and nuclear magnetic quantum numbers m_S and m_I. For small hyperfine interaction constants A, $E(m_S,m_I)$ is mainly given by the eigenvalues of H_1:

$$\begin{aligned} E_1(m_S,m_I)&=\langle m_S,m_I \,|\, H_1 \,|\, m_S,m_I\rangle \\ &=\mu_B g_e H m_S + A m_I m_S \; . \end{aligned} \tag{8a}$$

The term H_2 in Eq. (5b) is zero in first order, but provides second-order contributions to the spin energy of the form

$$\begin{aligned} E_2(m_S,m_I)=\left[\frac{A^2}{2\mu_B g_e H}\right]\{ m_S[I(I+1)-m_I^2] \\ -m_I[S(S+1)-m_S^2]\} \; . \end{aligned} \tag{8b}$$

From Eqs. (8a) and (8b), the ESR transition energies for an electronic spin with $S=\frac{1}{2}$ can be calculated as the difference of the energy E_1+E_2 for the $m_S=+\frac{1}{2}$ and $-\frac{1}{2}$ level as

$$\Delta E(m_I)=\mu_B g_e H + A m_I + \left[\frac{A^2}{2g_e\mu_B H}\right][I(I+1)-m_I^2] \; , \tag{9}$$

where each of the $2I+1$ possible values of $m_I=-I,-I+1,\ldots,+I$ occurs with equal probability. Thus, for an electronic spin $S=\frac{1}{2}$ the effect of the hyperfine interaction with a nuclear spin I is to split the single resonance transition occurring at an energy $\mu_B g_e H$ into $2I+1$ resonances of equal spectral weight occurring at the energies given by Eq. (9).

This equation will now be used for a discussion of the ESR hyperfine structure observed in *a*-Si:H and *a*-Ge:H samples doped with arsenic or phosphorus.[50] Typical spectra are shown in Figs. 5 and 6. First, Fig. 5 depicts the low-temperature ($T=40$ K) ESR spectrum of *a*-Ge:H doped with 1% PH_3. The spectrum covers a magnetic field range of 1000 G and is dominated by the resonance of electrons localized in weak Ge-Ge antibonding orbitals (conduction-band tail, $g=2.012$, peak-to-peak linewidth $\Delta H_{\text{p.p.}}=33$ G). In addition to this central resonance, two weak structures can be detected, occurring symmetrically at the high- and low-field side of the central resonance. The field splitting, ΔH, between these resonances amounts to 275 G, their linewidths to about 30 G. The symmetric

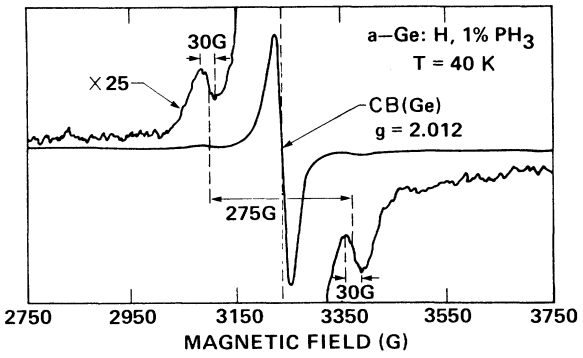

FIG. 5. Electron-spin-resonance spectra of phosphorus-doped a-Ge:H, showing the central conduction-band-tail resonance and the hyperfine-split line due to neutral phosphorus dopants for a doping level of 1% at $T=40$ K.

position and the equal intensities of these two additional signals is indicative of an electronic spin in hyperfine contact with a nuclear spin $I=\frac{1}{2}$ or $I=1$. (In the latter case the third hyperfine signal would be unobservable because of the much stronger central resonance.)

The upper part of Fig. 6 shows a similar behavior of the ESR spectrum in phosphorus-doped a-Si:H. Here, the splitting between the two satellites is $\Delta H=245$ G, with a peak-to-peak linewidth of about 60 G for both lines. Note

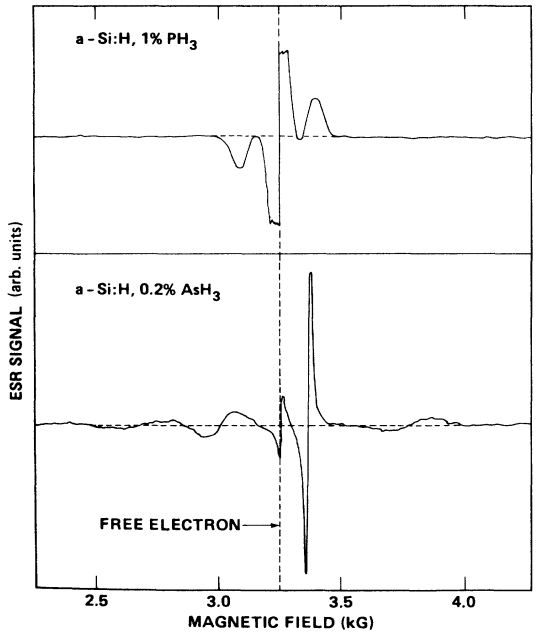

FIG. 6. Central conduction-band-tail resonances and donor hyperfine spectra in a-Si:H doped with phosphorus (upper half) and arsenic (lower half). The vertical dashed line indicates the position of the free-electron g value $g=2.0023$.

the small but distinct difference between the line shapes of the two hyperfine satellites. This difference is due to the no longer negligible contribution of the second-order term E_2 [Eq. (8b)] to the hyperfine structure. This point will be discussed in more detail below. As in a-Ge:H, the strong resonance seen near the free-electron position is due to electrons in conduction-band tail states experiencing no hyperfine interaction ($g=2.0044$, $\Delta H_{\text{p.p.}}=7$ G).

Finally, the lower part of Fig. 6 shows the ESR spectrum of a-Si:H doped with 0.2% AsH_3. Again, the conduction-band tail resonance is observed at the free-electron position, however, with a much reduced intensity as compared to phosphorus-doped material. Moreover, instead of two nearly symmetric hyperfine lines, four lines with different linewidths and amplitudes are obtained. Twofold integration over this spectrum shows, however, that the numbers of electronic spins associated with each of the four off-center resonances are equal within experimental accuracy. Hence it appears likely that these four lines are the hyperfine split states belonging to a nuclear spin $I=\frac{3}{2}$, the asymmetric shapes and positions being due to strong second-order contributions to the hyperfine interaction.

A comparison of the spectra in Figs. 5 and 6 with the list of nuclei in Table III leads to the conclusion that the nuclei responsible for the hyperfine splitting in phosphorus-and arsenic-doped samples are ^{31}P and ^{75}As, respectively. For the arsenic-doped material, this is safe to conclude, because ^{75}As is the only nucleus with $I=\frac{3}{2}$ that occurs with a large enough concentration to account for the density of hyperfine split electronic spins quantitatively. In the case of phosphorus-doped a-Si:H and a-Ge:H, on the other hand, the nuclei ^{1}H, ^{13}C, ^{14}N, and ^{15}N cannot be ruled out as the potential hyperfine centers *a priori*. In order to clarify this point, two additional experiments have been performed (see Fig. 7). First, the role of hydrogen can be checked by isotopic substitution with deuterium. The deuteron has a different spin ($I=1$) and a smaller nuclear moment ($0.857\mu_n$) than the proton, so that deuteration would drastically change any hyperfine structure due to ^{1}H. However, no difference is seen between the hyperfine lines of ^{31}P-doped a-Si:H and a-Si:D. Secondly, to investigate the role of impurity nuclei (C,N), a phosphorus-doped sample was deposited under otherwise identical conditions in an ultrahigh-vacuum (UHV) deposition system.[51] This is known to reduce the concentration of carbon and nitrogen in the amorphous film by 2 or 3 orders of magnitude, but, according to Fig. 7, has no effect on the density of hyperfine split states. Thus, it is clear that the donor nuclei ^{31}P and ^{75}As are responsible for the hyperfine splitting in Figs. 5 and 6.

For a quantitative analysis of these hyperfine spectra, we rewrite Eq. (9) with the help of the ESR resonance condition,

$$h\nu=g_e\mu_B H_0 \,, \tag{10}$$

where H_0 is the resonant field for an electron with g value g_e under the influence of a microwave $h\nu$. Expressing the hyperfine interaction constant A in terms of the magnetic field splitting $\Delta H=A/g_e\mu_B$, one obtains for the

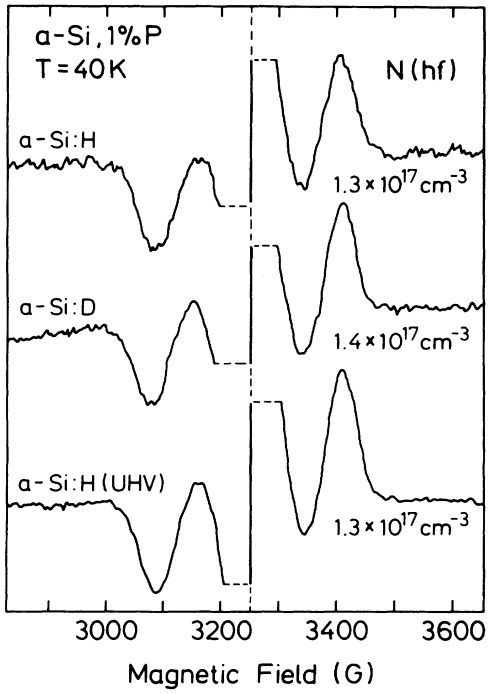

FIG. 7. Phosphorus hyperfine spectra in hydrogenated amorphous silicon (upper trace), deuterated amorphous silicon (central trace), and hydrogenated amorphous silicon prepared under UHV conditions (lower trace). N(hf) is the electron-spin density associated with the hyperfine spectra.

magnetic field position $H(m_I)$ of the $2I+1$ hyperfine lines:

$$H(m_I)=H_0-m_I\Delta H-[I(I+1)-m_I^2]\frac{(\Delta H)^2}{2H_0} . \quad (11)$$

The different terms in this expression correspond to the zero-, first- and second-order contribution of the hyperfine interaction to the position of the ESR resonances. In zero order, this position is given by the resonant field, H_0, of the free electron. Including the hyperfine interaction to first order leads to $2I+1$ lines shifted symmetrically with respect to H_0. This first-order approximation is usually sufficient for hyperfine splittings $\Delta H < 100$ G. Examples are the well-known donor-hyperfine spectra in crystalline silicon and germanium.[52–55] In cases where the hyperfine splitting ΔH becomes too large, the second-order term in Eq. (11) can no longer be neglected. The effect of this term is to destroy the symmetry of the hyperfine spectra with respect to H_0: each hyperfine line is shifted to lower magnetic fields, and the spacing between adjacent hyperfine lines increases from the low-field towards the high-field side of the spectrum. Indeed, when Eq. (11) is applied to the spectra in Figs. 5 and 6, the field position of all resonances (characterized by the zero-crossing points of the ESR derivative signal) can be accurately described by the following values for the splitting constant, ΔH:

$\Delta H = 275$ G for ^{31}P-doped a-Ge:H ,

$\Delta H = 245$ G for ^{31}P-doped a-Si:H ,

$\Delta H = 355$ G for ^{75}As-doped a-Si:H .

However, this does not provide an explanation for the observed line shapes of the various hyperfine lines. If we look at Eq. (11), this line shape could be influenced in two ways. First, the resonances in a-Si:H and a-Ge:H are known to be inhomogeneously broadened because of the g-value anisotropy.[31] This leads to a distribution of resonance fields H_0, rather than a well-defined value. According to Eq. (11) one would therefore expect a broadening of all hyperfine lines by approximately the same amount. Moreover, the g-value anisotropy and therefore the line broadening should be larger in a-Ge:H than in a-Si:H, because of the larger spin-orbit coupling constant. Although g-value anisotropy could explain the hyperfine line shapes in phosphorus-doped a-Ge:H, it is evident that a different mechanism must be responsible for the observed line shapes in a-Si:H. The second quantity in Eq. (11) which can influence the shape of the hyperfine lines is the splitting constant, ΔH. A distribution of possible splitting constants, again, will lead to a broadening of the hyperfine lines. In contrast to broadening by g-value anisotropy, however, the broadening due to a distribution of ΔH values will affect hyperfine lines corresponding to different quantum numbers m_I differently. This is evident from the mathematical form of Eq. (11).

Physical reasons for such a distribution of hyperfine splittings ΔH, or, equivalently, of hyperfine interaction constants A are, for example, an anisotropy of the hyperfine tensor, [**A**], or different degrees of localization for the electronic wave function [cf. Eqs. (6) and (7)]. We will postpone a more-detailed discussion of these possibilities until the end of this section. Here, we will assume for illustration that a Gaussian distribution of splittings ΔH exists:

$$P(\Delta H)\propto\exp\left[-4\ln 2\frac{(\langle\Delta H\rangle-\Delta H)^2}{W^2}\right] . \quad (12)$$

In Eq. (12), $P(\Delta H)$ is the (unnormalized) probability for the occurrence of a splitting ΔH, W is the full width at half maximum (FWHM) of the distribution, and $\langle\Delta H\rangle$ is the mean splitting already listed above. Equations (11) and (12) can now be used to fit the experimentally observed hyperfine spectra. The best fits are obtained for the following values of the parameter W:

$$W=\begin{cases}70\text{ G}, & ^{31}\text{P in } a\text{-Ge:H}\\ 165\text{ G}, & ^{31}\text{P in } a\text{-Si:H}\\ 150\text{ G}, & ^{75}\text{As in } a\text{-Si:H} .\end{cases}$$

The corresponding calculated spectra are shown in Fig. 8. Comparison with the measured spectra shows that the positions, widths, and relative amplitudes of all hyperfine lines are accurately reproduced by the simple model employed. Before addressing the physical significance of the two fitting parameters, $\langle\Delta H\rangle$ and W, we will first turn to

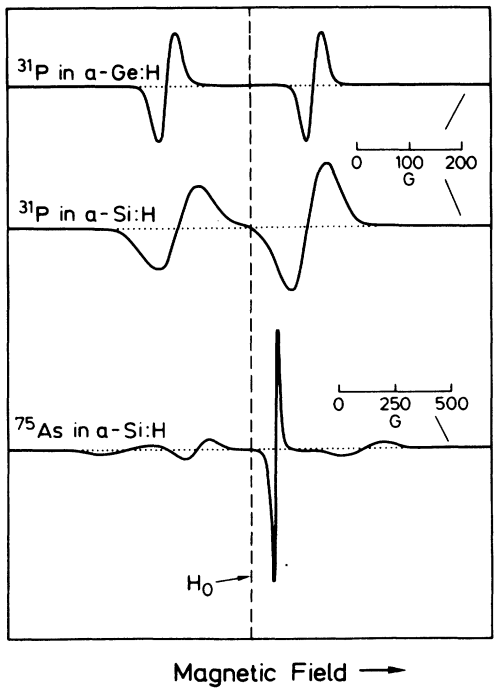

FIG. 8. Simulation of the ^{31}P and ^{75}As hyperfine spectra in a-Si: and a-Ge:H based on Eqs. (11) and (12) in the text. The dashed line at a field H_0 denotes the resonant field of a free electron.

a discussion of which microscopic electronic states are the origin of the observed hyperfine spectra.

Two general properties of the states in question are immediately obvious: (1) The states must be paramagnetic, i.e., containing an odd number of electrons, in order to account for the observation of a net spin in ESR; and (2) the electronic wave function Ψ_e of the unpaired electron must be strongly localized at the site of the dopant atom, in order to explain the strong hyperfine splitting observed. To be more quantitative, the wave function Ψ_e has to be of considerable s-like character, with an effective Bohr radius a smaller than the one measured for donor states in crystalline silicon and germanium. With the convention for the description of electronic states used in the Introduction, possible candidates for the hyperfine split electronic orbitals in phosphorus-doped samples are the electronic states denoted by P_2^0, P_3^+, P_3^-, and P_4^0. Of course, similar considerations are valid for the case of arsenic doping. In a simple tight-binding picture, the P_2^0 configuration corresponds to a phosphorus dangling bond state, where the wave function Ψ_e is derived from a nonbonding p orbital of the dopant atom. Similarly, the P_3^+ and P_3^- states are derived from holes or electrons localized in Si—P bonding and antibonding states of threefold-coordinated phosphorus atoms, respectively. In the two cases of P_2^0 and $P_3^{\pm}$, the hybridization state of the phosphorus atoms inside the a-Si matrix does not have to change significantly from the $2p^2p^3$ configuration of atomic phosphorus. In contrast, the realization of the fourth possible configuration of Ψ_e, P_4^0, requires a change of the hybridization from $3s^2p^3$ to $3(sp^3)^5$. In this case, the single electron responsible for the paramagnetic response occupies the sp^3-antibonding orbitals of a phosphorus atom bonded to four silicon atoms.

A crude estimate of the energies corresponding to these different paramagnetic states relative to the a-Si:H valence and conduction bands can be obtained from the level diagram in Fig. 9. This diagram is based on the atomic Hartree-Fock energies given in Table II and on approximate values of the Si—Si and Si—P bonding energy (2.5—3 eV). First, from the atomic levels the relevant hybrids are constructed. Then, the bonding and antibonding orbitals are derived, using the above bonding energies and, for simplicity, a symmetric bonding-antibonding splitting. The broadening of the silicon levels into valence and conduction bands via the intrasite interaction is also indicated. It can be seen from Fig. 9 that neither the nonbonding P_2^0 nor the bonding or antibonding P_3^+ or P_3^- state is likely to give rise to the hyperfine resonance observed in phosphorus-doped a-Si:H. This is due to the fact that the $3p$ orbital of P has nearly the same energy as the sp^3 hybrids of silicon. Hence, the P_3 states (bonding or antibonding) will occupy the same energy range as the Si valence and conduction bands, so that the species P_3^+ (hole in the P_3 bonding state) or P_3^- (electron in the P_3 antibonding state) should not occur in a thermal equilibrium situation. Rather, threefold-coordinated phosphorus (or arsenic) will be present in the neutral, diamagnetic, and nondoping P_3^0 (As_3^0) state.

As far as the P_2^0 state (phosphorus dangling bond) is concerned, the decision as to whether it could be the observed hyperfine-split defect in a-Si:H is somewhat less obvious. According to Fig. 9, the P_2^0 state is derived from a nonbonding $3p$ level of the phosphorus and occurs in the same energy range as the silicon dangling bond, Si_3^0. Therefore, it should not be observable in n-type a-

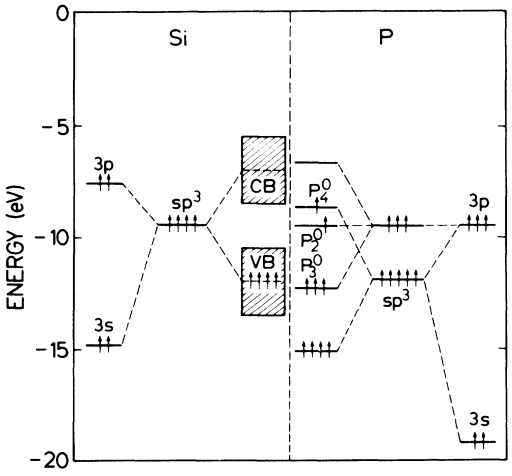

FIG. 9. Energy-level diagram for phosphorus donors in a-Si:H. See text for details.

Si:H, where the Fermi level is close to the conduction-band edge, unless the P_2^0 state has a larger positive correlation energy than the Si_3^0 defect. Additional arguments against the assignment of the hyperfine lines in phosphorus-doped *a*-Si:H to P_2^0 defects can be derived from the following observations.

(i) The hyperfine splitting measured in *a*-Si:H is much larger than that observed for PH_2 radicals [$\Delta H \approx 80$ G (Ref. 56)] or atomic phosphorus [$\Delta H \approx 20$ G (Ref. 57)]. This indicates that the states responsible for the hyperfine spectra have a larger admixture of *s*-like character to the spin wave function Ψ_e than the *p*-derived state of a PH_2 radical. (Note that electronic states with pure *p* character only contribute to the hyperfine tensor [**A**] in Eq. (5) via the anisotropic dipolar interaction between the electronic and nuclear spins. This interaction, however, is much smaller than the Fermi-contact interaction of *s*-like states described by Eq. (7).)

(ii) Paramagnetic states in amorphous arsenic and phosphorus, which are ascribed to As_2^0 and P_2^0, exhibit spin resonance signals which are distinctly different from the hyperfine spectra shown in Fig. 6.[58,59]

(iii) As will be shown in more detail in Sec. III, the hyperfine spectra are not observed in the thermal equilibrium ESR spectra of compensated (i.e., doped with equal amounts of boron and phosphorus) *a*-Si:H, but appear in the low-temperature light-induced (LESR) spectra. Again, this shows that the hyperfine-split electronic state is a shallow rather than a deep paramagnetic defect in *a*-Si:H.

This leaves only the P_4^0 state as the paramagnetic defect responsible for the hyperfine spectra in phosphorus-doped *a*-Si:H. According to Fig. 9, the observed spin state is derived from the sp^3-antibonding orbital of a fourfold-coordinated phosphorus atom. Indeed, this state satisfies all of the restrictions imposed by the experimental results. The P-Si antibonding character of the level explains its position close to the conduction-band edge and, therefore, the donor character of P_4^0. Moreover, the state is obviously paramagnetic and has sufficient *s* character to explain the magnitude of the observed hyperfine interaction. Last but not least, the obvious similarities between the hyperfine states introduced by *n*-type doping in amorphous and crystalline silicon and germanium also suggest a common nature of the underlying microscopic configurations.

According to Tables II and IV, the same arguments used for an explanation of the hyperfine spectra in phosphorus-doped *a*-Si:H should apply as well to the cases of arsenic-doped *a*-Si:H and to *a*-Ge:H doped with both phosphorus and arsenic. Indeed, this is in agreement with all experimental results shown so far. Moreover, in a series of articles,[62] Robertson has performed a detailed tight-binding modeling of *a*-Si and *a*-Si:H doped with various group-III and -V elements. As far as *n*-type doping is concerned, Robertson's results are in qualitative agreement with the crude picture presented in Fig. 9. Of special interest for the following are the theoretical predictions for the energy location of the P and As donor levels in *a*-Si:H with respect to the conduction-band mobility edge [$E_c - E(P_4) \approx 0.1$ eV, $E_C - E(As_4) \approx 0.3$ eV] as well as the disorder broadening of these levels (≈ 50 meV in both cases). However, before we will attempt a quantitative modeling of the donor wave functions in *a*-Si:H and *a*-Ge:H and a comparison to the theoretical predictions, we first would like to present additional experimental information concerning the dependence of the donor hyperfine spectra on doping level and temperature.

TABLE IV. Strength of selected bonds relative to the Si—Si bond (from Ref. 61).

Bond	Relative strength	Bond	Relative strength
B—B	0.88	B—H	1.03
Si—Si	1.00	Si—H	0.94
Ge—Ge	0.85	Ge—H	1.00
N—N	2.97	N—H	1.00
P—P	1.55	P—H	1.03
As—As	1.21	As—H	0.85

The dependence of the ESR parameters (hyperfine splitting, spin density, *g* value, and peak-to-peak linewidth, $\Delta H_{p.p.}$) for the two hyperfine lines in phosphorus-doped *a*-Si:H on the gas-phase doping level is summarized in Figs. 10(a)—10(d). Also included are hyperfine splitting and spin-density data for *a*-Ge:H. As seen in Fig. 10(a), the hyperfine splitting in both materials is independent of the doping level within the experimental accuracy of 10 G. Average values are $\Delta H = 275$ G in *a*-Ge:H and $\Delta H = 240$ G in *a*-Si:H. Figure 10(b) shows that the spin density associated with the hyperfine states increases sublinearly with the phosphine concentration in the plasma used for deposition. As indicated by the solid lines, the increase follows roughly a square-root power law, with signs of saturation for the highest doping levels ($> 10^{-2}$). An obvious reason for this saturation is the increasing probability for direct bonds between dopant atoms. (See also the results for arsenic-doped *a*-Si:H below.) As indicated by the left- and right-shaded symbols, the spin densities of the two ^{31}P hyperfine resonances in Fig. 10(b) have been plotted separately. Generally, similar spin densities are obtained for both lines, supporting the interpretation of the two resonances as a pair of hyperfine lines. Also included in Fig. 10(b) is the doping dependence of the spin density of electrons localized in the *a*-Si:H conduction-band tail (curve marked "CB"), which shows the pronounced saturation behavior already discussed in Sec. II B.

In Fig. 10(c), we have compiled the experimental values for the effective *g* value of the ^{31}P hyperfine center in *a*-Si:H. This effective *g* value is obtained by defining an effective resonance field $H_{0,\text{eff}}$ as the arithmetic average of the resonant fields for the low- and high-field hyperfine lines and calculating g_{eff} according to the resonance condition, Eq. (10):

$$g_{\text{eff}} = \frac{2h\nu}{\mu_B[H(m_I = -\frac{1}{2}) + H(m_I = +\frac{1}{2})]} . \tag{13}$$

Figure 10(c), then, suggests an average value of $g_{\text{eff}} = 2.006$. Because of the large hyperfine interaction, however, we should also include second-order contribu-

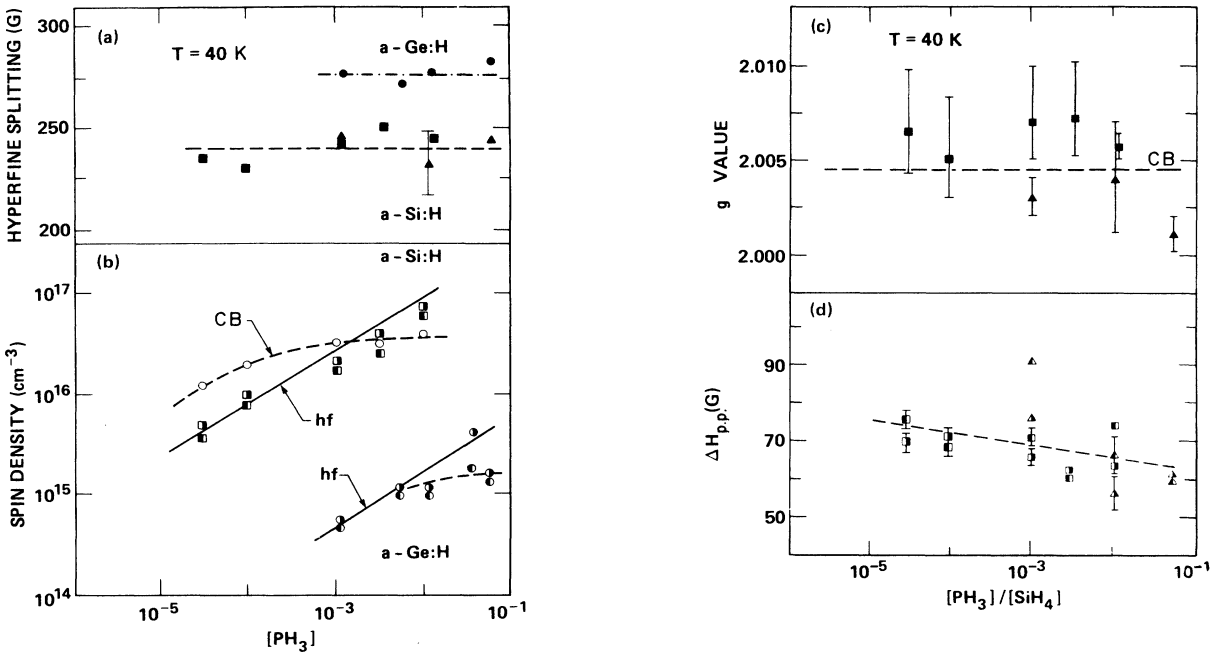

FIG. 10. ESR parameters for n-type a-Si:H and a-Ge:H as a function of phosphorus doping level. (a) Magnetic field splitting of the ^{31}P hyperfine lines. (b) Spin densities for the conduction-band-tail resonance (CB) and the neutral donors (hf). (c) Effective g value and (d) peak-to-peak linewidth in phosphorus-doped a-Si:H. Left- and right-shaded symbols in (b) and (d) refer to the low-field and high-field hyperfine lines, respectively.

tions to the hyperfine splitting. Following Eq. (11), we obtain for the ^{31}P resonance lines ($I=\frac{1}{2}$) a correction of the form

$$H_0 \rightarrow H_0 + \frac{(\Delta H)^2}{4H_0} \ . \tag{14}$$

With $\Delta H = 245$ G and $H_0 = 3255$ G (for an X-band microwave $\nu = 9.14$ GHz), this second-order correction to the g value of the ^{31}P donor wave function amounts to a 4.6-G shift of H_0 to higher fields, thus yielding

$$g(\mathrm{P}_4{}^0) = 2.003(\pm 0.002)$$

in a-Si:H. This has to be compared to a value of 1.998 50 in crystalline silicon.[53] Similarly, for ^{75}As the g value of the neutral donor state in a-Si:H is obtained as

$$g(\mathrm{As}_4{}^0) = 2.005(\pm 0.002) \ .$$

The corresponding value for crystalline silicon is 1.998 37.[53]

It is interesting to note that the g-shift $g - g_0$ (where $g_0 = 2.0023$ is the free-electron g value) for the neutral donor states has, within the given experimental accuracy, the opposite sign (positive) in amorphous compared to crystalline silicon. Most likely, this is due to the fact that the donor wave function in a-Si:H can no longer be approximated by a shallow, effective-mass state. Instead, spin-orbit coupling with the p-like states forming the top of the valence band appears to dominate the g shift, similar to the g value of the weak antibonding orbitals in the conduction-band tail ($g = 2.0044$). (For a more-detailed discussion of electronic g values in a-Si:H see Ref. 63.)

The peak-to-peak linewidth, $\Delta H_{\mathrm{p.p.}}$, of the phosphorus hyperfine spectra is shown in Fig. 10(d). As indicated by the dashed line, this linewidth decreases by about 10 G with increasing doping level. The variation of $\Delta H_{\mathrm{p.p.}}$ with doping level implies that the parameter W describing the width of the distribution of hyperfine splittings ΔH [see Eq. (12)] also decreases with doping.

The dependence of the spin density of shallow states (conduction-band tail and neutral donors) on the solid-phase dopant concentration in arsenic-doped a-Si:H is depicted in Fig. 11. For low doping levels ($< 4\times 10^{-2}$), the density of electrons in the conduction-band (CB) tail is constant at about 2×10^{15} cm^{-3}. The density of hyperfine-split, neutral As-donor electrons (hf), on the other hand, increases linearly with doping level up to a maximum value of 10^{17} cm^{-3}. For higher doping levels ($> 10^{-1}$), both ESR signals disappear quite rapidly, most likely because of the onset of alloying, i.e., an increasing probability of bond formation between two As atoms. A similar effect has also been observed in previous investigations.[64–66] A comparison of the data in Fig. 11 with the experimental results for phosphorus-doped a-Si:H in Fig. 10(b) shows that the density of occupied conduction-band-tail states is about an order of magnitude higher in P-doped a-Si:H. This result is consistent with the slightly higher Fermi energy in the latter material [cf. Fig. 2(a)]. As far as the neutral donor states are concerned, in both, phosphorus- and arsenic-doped samples, a maximum ESR

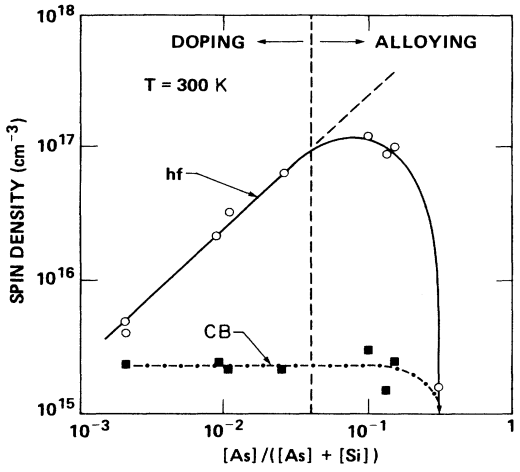

FIG. 11. Dependence of the neutral donor (hf) and conduction-band-tail (CB) ESR spin densities on the solid-phase dopant concentration in arsenic-doped a-Si:H at $T=300$ K.

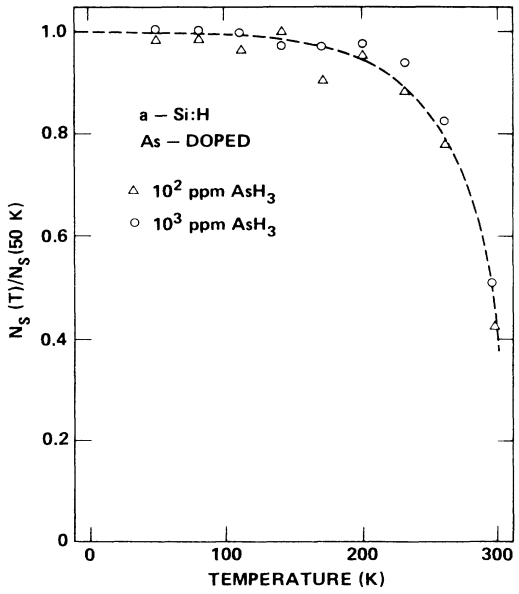

FIG. 13. Variation of the normalized neutral donor spin density in arsenic-doped a-Si:H with temperature for a gas-phase doping level of 10^{-4} (triangles) and 10^{-3} (circles).

spin density of about 10^{17} cm^{-3} is measured at the highest doping levels. However, the increase of the spin density with the solid-phase dopant concentration is faster for arsenic than for phosphorus doping.

Finally, in Figs. 12 and 13 we show the temperature dependence of the spin density for the neutral arsenic and phosphorus dopant states. For comparison, in Fig. 12 the temperature dependence of the conduction-band-tail spin density is given, as well. The hyperfine split donor resonances exhibit a constant spin density up to a temperature of about 200 K. Beyond this temperature, the spin density decreases quite rapidly. In analogy to crystalline silicon, we can interpret this behavior as the thermal ionization of the donor electrons out of the neutral dopants into the conduction band. The characteristic ionization temperature of $\simeq$200 K is much higher than in crystalline silicon ($\approx$30 K), due to the larger energy separation of the neutral donor states from the propagating conduction-band states ($\approx$200 meV in a-Si:H versus 50 meV in c-Si, see below). In contrast to the decreasing density of occupied donors, the number of spins in conduction-band-tail states shows a slight increase in the same temperature range. Possible explanations for this observation could be a partial recapture of thermalized donor electrons by the tail states or temperature-dependent changes in the probability for single occupancy of the tail state as discussed by Dersch *et al.*[28]

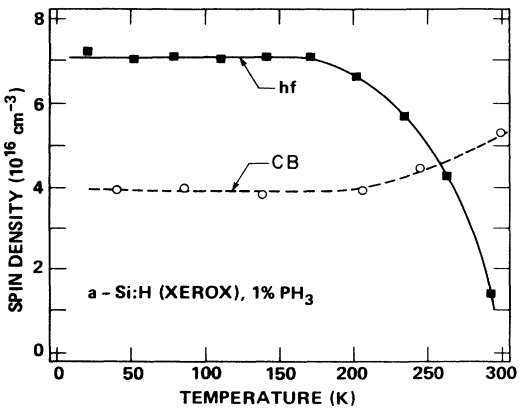

FIG. 12. Temperature dependence of the hyperfine (hf) and the conduction-band-tail (CB) spin densities in phosphorus-doped a-Si:H for a 1% gas-phase doping level.

2. *Discussion of experimental results*

Three qualitative conclusions concerning the donor states in a-Si:H and a-Ge:H can be drawn from the experimental results described above.

(i) The donor electrons in the amorphous phase are more localized than in the crystalline material, thus experiencing a stronger hyperfine interaction with the dopant nuclei.

(ii) In a-Si:H and a-Ge:H, a relatively broad distribution of donor levels rather than a well-defined level exists. This leads to a broadening of the hyperfine satellites due to corresponding variations of the hyperfine interaction, ΔH [cf. Eq. (12)]. The likely reason for this distribution of donor levels is the bonding disorder in the amorphous films.

(iii) As evidenced by the higher thermalization temperatures, the energy distance of the neutral donor levels from delocalized states (conduction-band mobility edge) in a-Si:H and a-Ge:H is larger than in the crystalline case.

In the following, we will analyze these points in terms of a more quantitative model for the electronic density of states close to the conduction-band edge. The various parameters of this model are defined in Fig. 14. The density N_{CB} of intrinsic band-tail states (Si—Si weak bonds) decays approximately exponentially with a slope of 35 eV^{-1} from the conduction-band mobility edge E_C, and reaches a minimum of $\approx 10^{15}$ cm^{-3} eV^{-1} at $E_C-0.3$ eV. Superposed is the distribution N_D of ionized and neutral donors D_4^+ and D_4^0, depicted in Fig. 14 for the case of a 1% gas-phase doping with phosphorus. At low temperatures, all electrons will condense into states below $E_F(0)$, the extrapolated Fermi energy at $T=0$. This energy is constant at $\approx E_C-0.15$ eV for phosphorus doping levels above 10^{-4} [cf. Fig. 2(a)]. The density of occupied donors and tail states is given by

$$n(D_4^0)=\int_{E_{min}}^{E_F(0)} N_D(E)dE \tag{15a}$$

and

$$n(\mathrm{CB})=\int_{E_{min}}^{E_F(0)} N_{CB}(E)dE\ , \tag{15b}$$

where $E_{min}\approx E_C-0.4$ eV is a suitable lower cutoff energy. Because of the exponential dependence of the density of states on energy close to E_C, most of the contribution to the integral densities n(CB) and $n(D_4^0)$ will come from the energy interval close to the Fermi level, $E_F(0)$. Since these are the states observed in ESR, the values of $N_{CB}(E)$ and $N_D(E)$ at the Fermi energy can be estimated from the measured spin densities of the conduction-band-tail resonance (CB) and the hyperfine (hf) split neutral donor signal, respectively [see Figs. 10(b) and 11]. Moreover, from the fact that the density of CB states increases with temperature, whereas the density of neutral donors decreases (Fig. 12), we have to conclude that the increase of $N_D(E)$ as a function of energy is slower than for $N_{CB}(E)$, as indicated in Fig. 14. This insures that, as the Fermi level shifts to lower energies and the electron distribution function broadens with increasing temperature, the fraction of electrons which are thermally excited into CB-tail states is always larger than the fraction of electrons excited into higher donor levels, i.e., a net charge transfer out of the neutral donor levels into the conduction-band-tail states occurs, as experimentally observed. (Note that the sum of the CB and hf spin densities in Fig. 12 is not constant, as expected, but decreases by about 30% at higher temperatures. Most likely, this is caused by spin-lifetime effects. Electrons close to the mobility edge have a very short spin-lattice relaxation time.[67] The resulting lifetime broadening of the ESR signal can become so large that, at high temperatures, such spins can no longer be detected.)

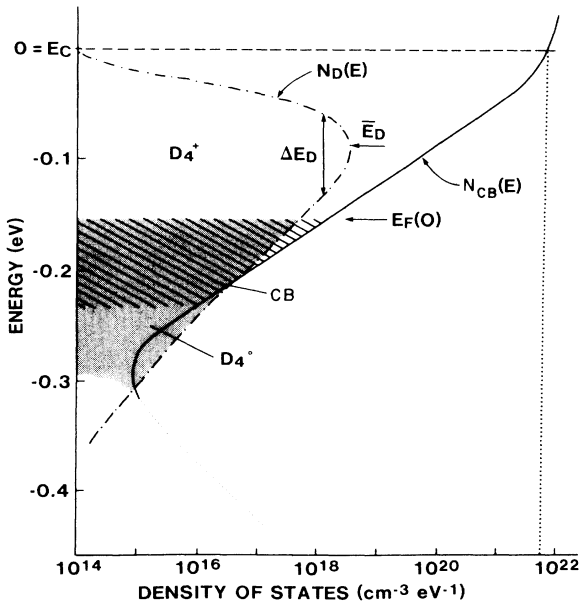

FIG. 14. Model for the electronic density of states near the conduction-band mobility edge E_C in n-type a-Si:H. $N_{CB}(E)$ and $N_D(E)$ refer to the partial DOS of the conduction-band tail and the donor band. E_D and ΔE_D denote the average donor energy and the donor-band FWHM, respectively. Occupied donor states and tail state (D_4^0, CB) are indicated by the shaded and cross-hatched regions, D_4^+ refers to ionized donor levels.

To the extent that deeper, compensating defects exist (dangling bonds, acceptors), a certain fraction of the electronically active donors will be in the ionized state, D_4^+, even at low temperatures, because the donor electrons have been trapped by these compensating levels. Actually, in doped a-Si:H and a-Ge:H the large majority, about 90%, of all donors are compensated by dangling-bond states. We will discuss this point in more detail in Sec. II D. For our model in Fig. 14 this means that the ESR hyperfine lines due to the neutral donor states, D_4^0, observe only the low-energy tail of the donor density of states, $N_D(E)$. About 10 times more unoccupied donors are present above the Fermi energy

$$n(D_4^+)=\int_{E_F(0)}^{E_{max}} N_D(E)dE \gg n(D_4^0)\ . \tag{15c}$$

Again, E_{max} is a suitable upper cutoff energy, with $E_{max}\approx E_C$ in phosphorus-doped a-Si:H. Unfortunately, the magnitudes and the temperature dependences of the conduction-band-tail and the donor spin resonance signals are not sufficient to completely determine the donor density of states, $N_D(E)$. Nevertheless, some estimates of the average donor energies, E_D, and of the width, ΔE_D, of the donor distribution can be obtained from the experimental values for $E_F(0)$ and the densities n(CB), $n(D_4^0)$, and $n(D_4^+)$. In Table V these experimental data and estimates for E_D and ΔE_D have been compiled for arsenic and phosphorus in a-Si:H and a-Ge:H. Also, theoretical estimates by Robertson[62] have been included for comparison. For the case of phosphorus in a-Si:H, calculations and experimental estimates are in excellent agreement placing the donor level at $E_C-0.1$ eV with a characteristic width of 50—100 meV. Both, experiments and calculations indicate that $N_0(E)$ for arsenic in a-Si:H is shifted to lower energies. The theoretical result of E_C-300 meV for the arsenic donor energy, however, is not consistent with the experimental data, which suggest that E_D is only shifted by 50 meV to lower energies, placing the arsenic donor at $E_C-0.15$ eV. This 50-meV shift explains the

TABLE V. Experimental and theoretical values for the donor density of states in a-Si:H and a-Ge:H. $E_F(0)$ is the Fermi-level position below E_C at low temperatures. n(CB), $n(D_4^0)$, and $n(D_4^+)$ are the densities of occupied tail states, neutral donors, and ionized donors, respectively. E_D denotes the average donor energy below E_C, and ΔE_D the width of the donor band (cf. Fig. 16). Experimental values are given for a 1% solid-phase doping level. Theoretical values have been taken from Ref. 62.

	a-Si:H P	a-Si:H As	a-Ge:H P
$E_F(0)$ (meV)	-150	-200	-250
n(CB) (cm^{-3})	4×10^{16}	2×10^{15}	1×10^{17}
$n(D_4^0)$ (cm^{-3})	7×10^{16}	4×10^{16}	2×10^{15}
$n(D_4^+)$ (cm^{-3})	2×10^{18}	1×10^{18}	$\approx2\times10^{18}$
E_D (meV)			
Expt.	≈-100	≈-150	≈-100
Calc.	-100	-300	
ΔE_D (meV)			
Expt.	≈100	≈100	
Calc.	50	50	

larger distance of E_F from E_C generally observed in arsenic-doped material, as well as the significantly smaller density of occupied band tail states (CB), compared to phosphorus-doped samples.

As far as phosphorus donors in a-Ge:H are concerned, no similar calculations have been performed so far. From the experimental data we can estimate that the donor level should be at $\approx E_C-0.1$ eV, similar to a-Si:H. The main difference between a-Ge:H and a-Si:H appears to be a larger density of dangling bonds and a smaller slope of the conduction-band tail (30 eV^{-1} in a-Ge:H versus 35–40 eV^{-1} in a-Si:H; see Ref. 31 and Fig. 4). This leads to the lower Fermi-level position in a-Ge:H, thus leaving fewer donor levels occupied.

Unfortunately, the ESR data do not permit us to draw more precise conclusions concerning the majority of the donor levels than those listed in Table V, since most of the donors are ionized and therefore diamagnetic. However, a little more can be said about the wave function of the occupied, neutral donors by analyzing the observed hyperfine spectra. The isotropic hyperfine interaction, $\Delta H(S)$, between the nucleus and the $3s$ ($4s$) electron of a ^{31}P (^{75}As) atom amounts to 3630 G (3420 G), whereas the anisotropic splitting due to a pure atomic p orbital is much weaker, $\Delta H(p)=100$ and 90 G, respectively.[68] If we express the donor wave function $\Psi_e(r)$ near the dopant nucleus as a linear combination of atomic $|s\rangle$ and $|p\rangle$ orbitals,

$$|\Psi_e\rangle=\eta(\alpha|s\rangle+\beta|p\rangle),\quad \alpha^2+\beta^2=1\ , \tag{16}$$

where η is the fraction of the total wave function localized at the donor atom, we can approximate the resulting hyperfine splitting ΔH by

$$\Delta H=\eta^2\alpha^2\Delta H(s)+\eta^2\beta^2(3\cos^2\theta-1)\Delta H(p)\ . \tag{17}$$

In Eq. (17), θ is the angle between the external magnetic field and the direction of the p orbital. In a disordered film, the average hyperfine splitting is, therefore

$$\Delta H=\eta^2\alpha^2\Delta H(s)\ . \tag{18}$$

The anisotropic term in Eq. (17) will result in a distribution of hyperfine splittings around this average value (powder pattern) with a width $W(p)$ given by

$$W(p)\approx3\eta^2\beta^2\Delta H(p)\ . \tag{19a}$$

A second possible reason for a distribution of hyperfine splitting in a-Si:H and a-Ge:H is the existence of a distribution $\delta(\eta^2\alpha^2)$ for the localization and/or hybridization of the donor wave function. The width $W(s)$ of such a distribution can be expressed as

$$W(s)=\delta(\eta^2\alpha^2)\Delta H(s)\ . \tag{19b}$$

Since the atomic splittings $\Delta H(s)$ and $\Delta H(p)$ are known, we can use the experimental results for ΔH and W listed in the preceding section to estimate the localization and the s- or p-character of the donor wave function in terms of the coefficients η^2 and α^2 (or $\beta^2=1-\alpha^2$). This comparison shows that two different types of wave functions are compatible with the ESR hyperfine data. The corresponding parameters are listed in Table VI for the different donors in a-Si:H and a-Ge:H. The type-I wave function is obtained by assuming that the experimentally observed width W of the distribution of hyperfine splittings is due to a powder pattern according to Eq. (19a). Because the experimental width W is of the order of the atomic anisotropic splitting, $\Delta H(p)$ (≈100 G), the type-I wave function has to be strongly localized and mostly p type in character. In contrast to this, the wave functions of type II are strongly delocalized and s-like, with a distribution of $\eta^2\alpha^2$ values of width $\delta(\eta^2\alpha^2)$ calculated from Eq. (19b).

TABLE VI. Parameters for possible donor wave functions of phosphorus and arsenic in amorphous silicon and germanium. η^2 denotes the fraction of the donor wave function localized at the dopant atom, α^2 the degree of s character. $\delta(\eta^2\alpha^2)$ is the width of the distribution of $\eta^2\alpha^2$ calculated from Eq. (19b).

		Type I		Type II		
Host	Donor	η^2	α^2	η^2	α^2	$\delta(\eta^2\alpha^2)$
Si	P	0.62	0.11	0.07	≈1	0.045
Si	As	0.66	0.16	0.10	≈1	0.044
Ge	P	0.31	0.25	0.08	≈1	0.019

Unfortunately, on the basis of the ESR hyperfine spectra alone it is not possible to decide which of the wave functions in Table VI gives a better description of the donor states in amorphous silicon and germanium. Moreover, in the case of a hyperfine line broadening due to a distribution of localization lengths or hybridization changes, according to Eqs. (18) and (19b) only the products $\eta^2\alpha^2$ and $\delta(\eta^2\alpha^2)$ can be determined from the hyperfine spectra, so that the localization parameter η^2 remains undetermined within the limits given in Table VI, as long as no additional information is taken into account. To this end, we first note that, generally, the effective Bohr radius, a, of the envelope of a bound state should decrease monotonically with the binding energy as approximately

$$a \propto |E_\infty - E|^{-1/2} \tag{20}$$

where $|E_\infty - E|$ is the energy difference between the energy E of the state and the nearest energy, E_∞, at which delocalization occurs ($a \rightarrow \infty$, e.g., the band edges in crystalline materials or the mobility edges in amorphous semiconductors). Thus, according to Table V, P_4^0 in a-Ge:H ($|E_\infty - E| \approx 250$ meV) should be more localized than P_4^0 in a-Si:H ($|E_\infty - E| \approx 150$ meV) whereas Table VI shows the opposite behavior for the wave functions of type I. Also, the η^2 and α^2 values of the type-I orbitals are quite similar to those recently determined for the dangling-bond defects in a-Si:H from ^{29}Si hyperfine measurements.[69] This means that the type-I orbitals can be viewed as P or As "dangling bonds," with energy levels close to midgap than those listed in Table V. Ishii *et al.*[70] have performed tight-binding calculations for the type-I orbitals (called "weak Si—P bonds" in their article) and, indeed, obtained an energy level at $E_c - 0.5$ eV for an essentially dangling bondlike wave function with a large positive correlation energy. However, these properties are in variance with most of the experimental results of the present study, especially the strong temperature dependence of the hyperfine spectra (Figs. 12 and 13). Finally, according to the introductory discussion in Sec. I, it is difficult to see microscopically why an essentially threefold-coordinated donor atom should remain in the paramagnetic, sp^3 hybridized state corresponding to a type-I wave function, rather than relax to the energetically favorable diamagnetic D_3^0 state. Taking all these points into account we feel that it is quite safe to conclude that orbitals of type I do not provide a satisfactory explanation for the observed hyperfine states.

On the other hand, the wave functions of type II in Table VI match quite accurately our microscopic picture of neutral donor states. The small η^2 values of ≈ 0.1 indicate that this wave function is considerably delocalized, similar to donor orbitals in crystalline Si and Ge and consistent with the shallow nature of the hyperfine states. Furthermore, the donor electron can be pictured as occupying the four sp^3 antibonding orbitals of a fourfold-coordinated donor atom with equal probability, so that the p-orbital contributions average to zero and the wave function is nearly s-like in the vicinity of the nucleus ($\alpha^2 \approx 1$). This being the case, we can calculate the donor electron probability at the nucleus, $|\Psi_e(0)|^2$, directly from the average hyperfine splitting ΔH [cf. Eq. (7)]. In Table VII, the experimental values are listed together with the corresponding values for crystalline silicon and germanium. Assuming a similar shape for the envelope of a donor state in crystalline and amorphous material, it follows from Eq. (6) that the effective Bohr radius a of the donors should scale like

$$a \propto [|\Psi_e(0)|^2]^{-1/3} . \tag{21}$$

Since $|\Psi_e(0)|^2$ is larger in a-Si:H and a-Ge:H than in crystalline Si and Ge by about 1 order of magnitude, the amorphous donor orbitals should be roughly 2 times more localized. The effective radii of 9—10 Å listed in Table VII were obtained by scaling the radii of As and P donors in crystalline silicon according to Eq. (21). The crystalline Ge donor radii are less suitable for scaling because of their extremely small donor ground-state energy [≈ 12 meV (Ref. 48)]. It should be noted that the present results are in very good agreement with previous estimates for the localization length of electrons in the conduction-band tail from luminescence experiments.[17]

The determination of the localization length, a, for the donor states close to the conduction-band mobility edge in a-Si:H and a-Ge:H via the hyperfine interaction allows us to address a question which is of considerable importance for many electronic properties of these materials, namely the dependence of the localization length on energy position in the mobility gap. For this purpose we have plotted in Fig. 15 the effective Bohr radii of various states in amorphous and crystalline silicon and germanium versus the energy depth, $|E_\infty - E|$ of these steps. The feature common to all of the data points in Fig. 15 is that the effective radii have been calculated from ESR measurements of the hyperfine interaction strength, rather than from a macroscopic quantity depending in a more or less complicated way on the localization length. Included in

TABLE VII. Experimental values for $|\Psi_e(0)|^2$ and the effective Bohr radii a of donors in crystalline and amorphous silicon and germanium. Values for crystalline material are from Refs. 48, 53, and 55.

		$\lvert\Psi_e(0)\rvert^2$ (Å^{-3})		a (Å)	
Host	Dopant	Crystalline	Amorphous	Crystalline	Amorphous
Si	P	0.43	2.5	16.7	10±1
Si	As	1.73	8.6	15.2	9±1
Ge	P	0.22	2.9	31.8	9±1
Ge	As	0.85		29.8	

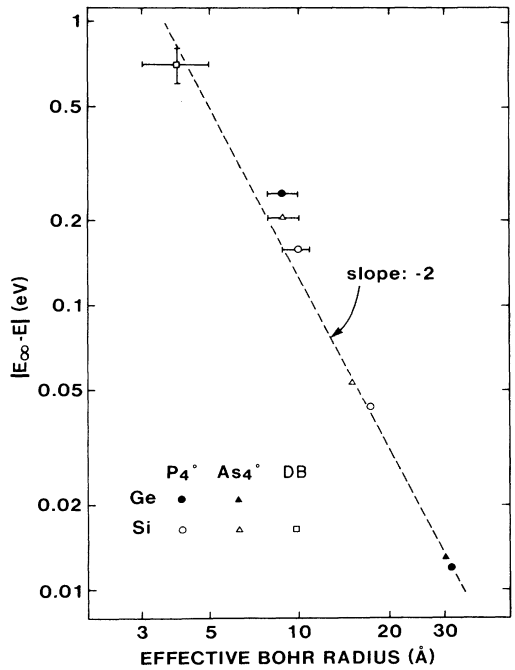

FIG. 15. Dependence of the effective Bohr radius on the defect binding energy, $|E_\infty - E|$, for various paramagnetic defects in amorphous and crystalline silicon and germanium, as determined from ESR hyperfine measurements. (P_4^0, As_4^0: neutral donor levels; DB: dangling-bond defect). The dashed line indicates the scaling behavior of Eq. (20).

Fig. 15 are the radii of As and P donors in crystalline and amorphous Si and Ge listed in Table VII, as well as the experimental value for the dangling-bond defect in *a*-Si:H.[69] The dependence predicted by the simple bound state equation (20) is indicated as a dashed line. It is quite surprising that the experimental results are in very good agreement with Eq. (20) over nearly 2 orders of magnitude in energy, spanning the range from the large donor orbitals in crystalline Ge to the atomic-like orbital of a dangling bond defect in *a*-Si:H. Thus, using Eq. (15) we can, for example, estimate the localization length of valence-band-tail states in *a*-Si:H or of dangling bonds in *a*-Ge:H to about 6—8 Å. Moreover, the same figure can be used to calculate the energy range occupied by the neutral donor states in *a*-Si:H and *a*-Ge:H (shaded region below E_F in Fig. 14) from the width W of the hyperfine interaction distribution. By relating the energy of a donor state to its hyperfine splitting via Eqs. (18)—(21), we find that the P and As donors in *a*-Si:H and the P donors in *a*-Ge:H occupy an energy range of approximately 70, 60, and 40 meV, respectively, below $E_F(0)$. This result is also in qualitative agreement with the total numbers D_4^0 of occupied donor states listed in Table V, which are largest for phosphorus-doped Si and smallest for phosphorus-doped Ge.

3. *Acceptor states*

P-type doping of *a*-Si:H and *a*-Ge:H is usually achieved by using boron as the acceptor. However, very little is known about these boron acceptor levels. In particular, no direct observation of these states with ESR has been possible so far. The reason for this can be understood by the schematic energy diagram in Fig. 16, which shows that the sp^2 and the sp^3 hybrids of a boron atom have nearly the same energy as the sp^3 hybrid of a silicon (or germanium) atom. Hence, when B is bonded inside an *a*-Si:H or *a*-Ge:H film, the boron bonding orbitals will occupy roughly the same energy range as the Si (or Ge) valence band. As a result, the neutral, paramagnetic acceptor state, B_4^0, can always capture an electron from energetically higher Si-Si (Ge-Ge) bonding states and achieve the ionized, diamagnetic B_4^- charge state, even at very high boron doping levels. Again, a more accurate tight-binding calculation for the energy of the B_4 states has been carried out by Robertson,[62] which also indicates that the fourfold-coordinated boron levels should lie very close to E_V. Therefore, microscopic information about the nature of the acceptor states is difficult to obtain experimentally. The result that fourfold-coordinated boron does not directly introduce observable defects in the mobility gap of *a*-Si:H is also corroborated by light-induced ESR measurements in compensated samples, which will be described in Sec. III in more detail.

An interesting question is whether boron in other than fourfold coordination introduces defect states in the gap of *a*-Si:H. From theoretical considerations, Robertson argued that the negative and the neutral charge state of threefold-coordinated boron, B_3^0 and B_3^- should form deep defect levels.[62] Since threefold-coordinated states account for most of the boron in a doped sample (see our discussion of the doping efficiency in Sec. IV), this would mean that about 10^{20} cm^{-3} boron-related defects should occur in a sample with 1% doping level. This is clearly in contradiction with the bulk of the available experimental evidence. There is, however, some indication for boron-related effects on the electronic density of states in the valence-band tail of amorphous silicon,[72,73] which could

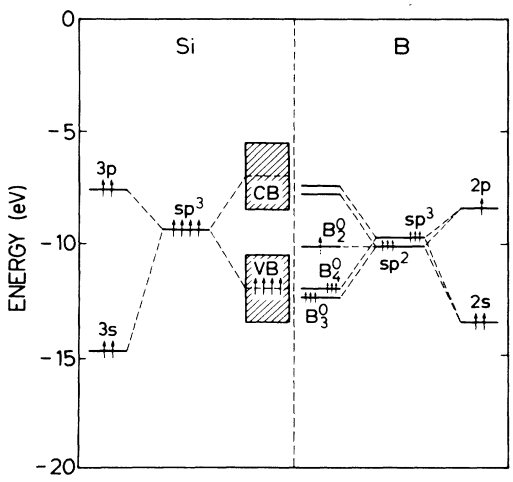

FIG. 16. Schematic energy-level diagram for boron-related electronic states in *a*-Si:H.

be caused either by additional defects or by doping-induced disorder broadening of the tail, for example due to changes of hydrogen bonding. One possibility for an additional defect state is the nonbonding orbital of a B_2^0 configuration which, according to Fig. 16, might occur near the *a*-Si:H valence-band edge.

D. Doping-induced changes of deep defect levels

As has already been pointed out above, doping of *a*-Si:H or *a*-Ge:H does not only introduce shallow acceptor or donor states, but can also lead to doping-induced changes of the electronic density of states near the center of the gap, i.e., changes in the density of deep defect levels. For the case of boron, we have already discussed the possibility that such states might be directly related to the dopant atoms themselves. The experimental evidence for this, however, is still rather uncertain. A second possibility is that the doping process leads to changes in the density of deep defects intrinsic to the amorphous network, i.e., of dangling-bond states.

The first direct proof of doping-induced changes in the dangling-bond density of states came from measurements of the luminescence intensity and from light-induced electron-spin-resonance (LESR) experiments in doped *a*-Si:H.[40] The dangling-bond levels near midgap act as efficient recombination centers and, hence, quench the radiative recombination processes leading to the tail-to-tail luminescence of *a*-Si:H at 1.3 eV. Therefore, the intensity of this luminescence band at a fixed temperature decreases with an increase of the total dangling-bond density, *N*. Moreover, LESR provides a direct proof for the fact that the doping-induced defects near midgap actually are dangling bonds.

An independent test of the luminescence and LESR has been provided by subgap absorption measurements. In these experiments, the weak absorption resulting from optical transitions out of the valence band into dangling-bond states and/or from the dangling bonds into the conduction band is detected. The defect absorption leads to an absorption band superposed on the band-to-band transitions, and the intensity of this band provides again a direct measure of the dangling-bond density.[74] For *a*-Si:H, the dangling-bond densities determined by the various techniques mentioned above agree reasonably. In doped *a*-Ge:H, luminescence measurements are much more difficult because of the higher intrinsic dangling-bond density and the smaller band gap, so that subgap absorption measurements are probably more reliable in this material.

So far, no subgap absorption measurements for arsenic-doped amorphous silicon have been reported in the literature. In Fig. 17, we show, therefore, some absorption spectra for the arsenic-doped samples used in this study. The doping levels are given in terms of solid phase concentrations of As, and correspond to arsenic plasma concentrations of 1.8×10^{-5}, 1×10^{-4}, and 1×10^{-3}, respectively. An absorption curve for *a*-Si:H with a 1% phosphine dopant gas concentration is also shown for comparison (dashed curve). Clearly, the subgap absorption (photon energies <1.5 eV) increases by nearly 2 orders of magnitude with increasing doping. Using the procedure by Jackson and Amer,[74] the absorption curves can be used to calculate the density of doubly occupied dangling bonds as a function of arsenic doping level. The results are shown in Fig. 18 (open circles), indicating an increase of the dangling-bond density from 10^{17} cm^{-3} to 2×10^{18} cm^{-3}. Also shown in Fig. 18 is the density of shallow states as determined by ESR and charge sweep

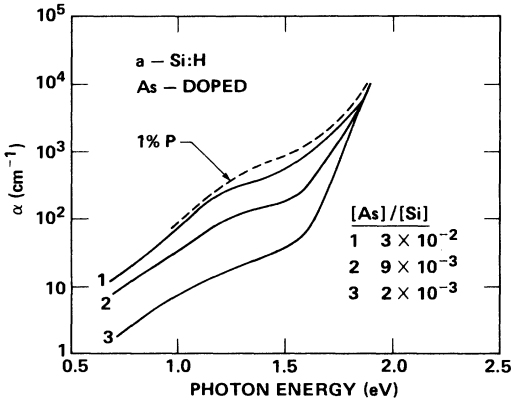

FIG. 17. Optical-absorption spectra measured by photothermal deflection spectroscopy of arsenic-doped *a*-Si:H. Arsenic concentrations in the deposited film are indicated. The dashed curve shows the absorption of *a*-Si:H doped with 1% phosphorus for comparison.

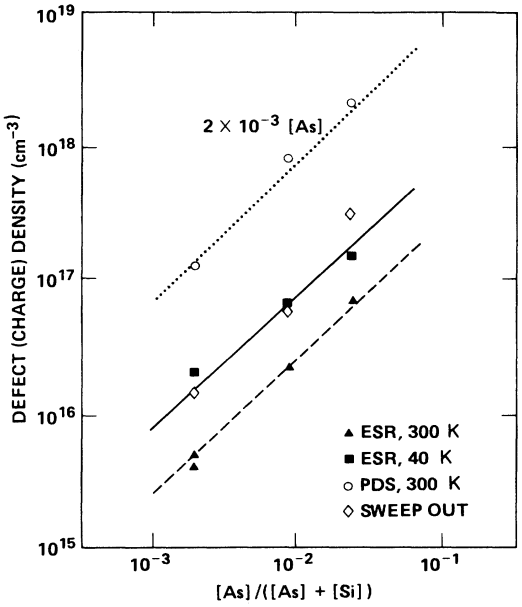

FIG. 18. Density of deep (open circles) and shallow states (all other symbols) as a function of solid-phase arsenic concentration. See text for details. The dotted line indicates a constant doping efficiency of 2×10^{-3} for arsenic with respect to the solid-phase dopant concentration.

out. Note that both, dangling bonds and shallow states, increase linearly with the solid-phase doping level. This is to be contrasted by the behavior of phosphorus-doped material, where both densities increase roughly with the square root of the doping level.[75] For a better comparison, we have compiled the dependence of the dangling-bond density on the gas-phase doping level for diborane, phosphine, and arsine in *a*-Si:H and *a*-Ge:H in Fig. 19. All experimental points were obtained by subgap absorption measurements and, except for the case of arsenic doping, were taken from already published work.[74,76] A discussion of these results will be deferred until Sec. IV. Here, we only would like to call the attention of the reader to the following points.

(i) For doping levels above 10^{-5}, the dangling-bond density in doped *a*-Si:H is at least an order of magnitude higher than the corresponding density in undoped *a*-Si:H. Boron and phosphorus samples exhibit an increase of the dangling-bond density as the square root of the gas-phase doping level, whereas this increase is faster for arsenic-doped material.

(iii) In contrast, doped *a*-Ge:H shows a dangling-bond density which is high and approximately independent of doping.

Finally, Fig. 20 shows a similar compilation for the density of shallow states (tail states plus occupied donor levels). Generally, the density of occupied shallow states is about an order of magnitude smaller than the dangling-bond density at the same doping level. Note also that the shallow state densities for boron-doped *a*-Si:H and *a*-Ge:H are very similar, whereas large differences are observed for the case of phosphorus doping. This reflects again the differences between the electronic density of states in the upper half of the mobility gap in the two materials (cf. Fig. 4).

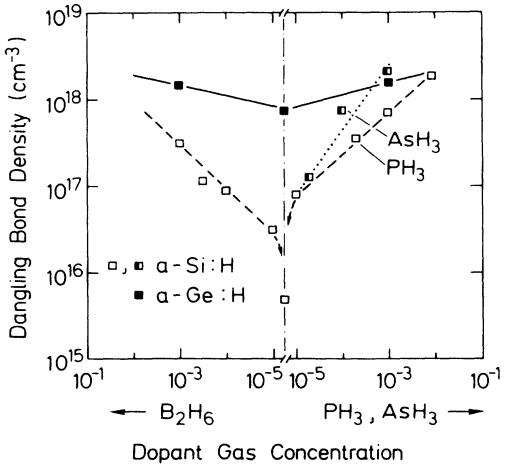

FIG. 19. Dangling-bond defect densities determined by photothermal deflection spectroscopy in *a*-Si:H and *a*-Ge:H doped with P, As, and B as a function of the dopant-gas concentration in the deposition plasma.

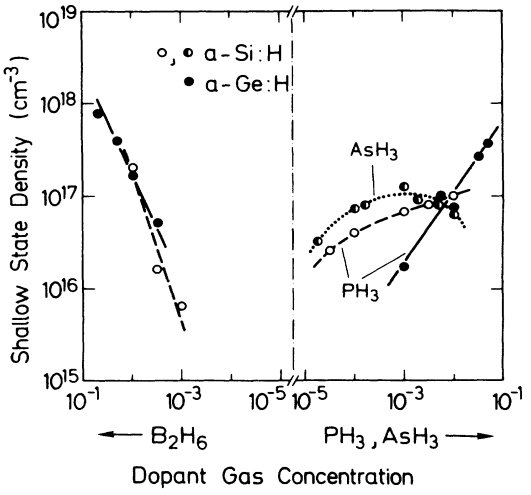

FIG. 20. Density of shallow states (band tail states and neutral donors) in *a*-Ge:H and *a*-Si:H measured with electron-spin resonance as a function of dopant-gas concentration.

III. COMPENSATED AMORPHOUS SILICON

So far, we have discussed the case of amorphous silicon or germanium containing only one type of dopant atoms. For a complete understanding of the doping process, however, it is desirable also to study the case of compensated material, i.e., samples containing both donor and acceptor atoms. This allows us to distinguish between doping effects which are related to the position of the Fermi level in the mobility gap, and those which depend on the presence of the impurity atoms. Only a few investigations have dealt with the electronic properties of compensated *a*-Si:H in detail. For the purpose of this discussion, we will use results published in references 40, 74, 77 and 78. More references can be found in these articles.

Compensated *a*-Si:H is easily prepared by adding both PH_3 and B_2H_6 simultaneously to the deposition plasma. Nominal compensation is achieved when the partial pressures of these gases are approximately equal. Quite interestingly, an analysis of the incorporation efficiency of P and B from such a gas mixture has shown that the solid phase concentrations of these two dopants tend to equalize, despite significant differences in the respective gas-phase concentrations. This fact has been interpreted as an indication for incorporation primarily via formation of P-B complexes already in the glow-discharge plasma.

Street, Biegelsen, and Knights have performed a rather extensive investigation of compensated *a*-Si:H using luminescence and electron-spin resonance. The luminescence intensity was observed to peak close to nominal compensation, indicating that the doping-induced increase of dangling-bond defects seen in the case of singly doped material does not occur in compensated samples (cf. Sec. II D). Also, with increasing compensation level (i.e., the same increase in boron and phosphorus doping level) the luminescence peak position shifted continuously from

about 1.4 eV in undoped material to about 1.0 eV at a compensation level of $[PH_3]=[B_2H_6]=10^{-3}$. On the basis of these results it was suggested that new states above the valence-band tail are introduced by compensation. The ESR experiments performed in the same study confirmed the absence of doping-induced dangling bonds in compensated *a*-Si:H. Using light-induced ESR (LESR), it was also found that nominally compensated samples exhibit a large density of optically excited holes trapped in the region of the valence-band tail ($\approx 5\times 10^{17}$ cm^{-3}), but no corresponding LESR signal of electrons in conduction-band-tail states was observed.

The results given in Ref. 40 were further corroborated by subband-gap absorption studies of Jackson and Amer.[74] In compensated *a*-Si:H, the absorption band due to dangling-bond defects was largely reduced, and at the same time the exponential absorption region due to tail-to-tail transitions was shifted to lower energies and broadened by about 0.2 eV, again indicating the existence of new states close to one of the band tails.

In order to further clarify the origin of these additional states in compensated material, recently time-of-flight and photoinduced absorption experiments have been performed. Marshall *et al.*, have used time-of-flight experiments to study the dependence of the electron and hole drift mobilities on compensation.[77] They found a decrease of the hole and electron drift mobilities by 2 orders of magnitude for a compensation level of $[PH_3]=[B_3H_6]=10^{-4}[SiH_4]$ relative to the undoped material, and interpreted this result as a corresponding increase of carrier trapping in compensation-induced defects near both band tails. In addition, the temperature dependence of the drift mobilities indicated an increase of the carrier trap depth from 0.1 to 0.35 eV for electrons and from 0.35 to 0.6 eV for holes. Formation of B-P complex pairs was suggested as the most likely explanation for these experimental results.

Finally, a study of the trapping and recombination dynamics in compensated *a*-Si:H was performed by Thomsen *et al.* using time-resolved photoinduced absorption measurements.[78] These authors concluded that the dopant states play an important role in the initial carrier trapping on a picosecond timescale, but that the recombination processes occurring at longer times (>10 ns) are very similar to those in undoped material.

A. New ESR results

For nominally compensated *a*-Si:H, the Fermi level is close to the center of the mobility gap and, therefore, the observed equilibrium ESR signal is that of the neutral silicon dangling bonds, Si_3^0, at $g=2.0055$. Unlike for the case of single boron or phosphorus doping, the dangling-bond density in compensated *a*-Si:H remains at the low value of undoped material. This is demonstrated in Fig. 21, where the intensity of the dangling-bond ESR signal of various samples (sample size: 5 μm$\times$1 cm$\times$0.5 cm) is shown as a function of the compensation level. In the stable, annealed state of the material, a constant number of dangling-bond spins is observed, corresponding to a defect density of $\approx 4\times 10^{15}$ cm^{-3}. This insensitivity of the

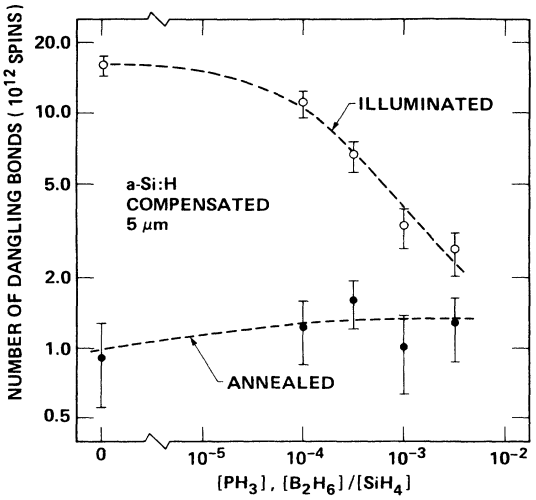

FIG. 21. Total number of dangling-bond spins in compensated *a*-Si:H as a function of compensation level. (Sample volume 5 $\mu m\times 0.5$ cm^2.) Solid circles refer to the annealed, stable state of *a*-Si:H; open circles to the state after prolonged illumination with intense light.

dangling-bond density to the compensation level is in agreement with previous results mentioned in Sec. III A. Also shown in Fig. 21 is the ESR signal intensity after light-induced degradation of the samples. A discussion of the observed behavior, i.e., an increasing stability with compensation, will be deferred until the next section.

Because of the small dangling-bond density in undoped or compensated samples, low-temperature illumination results in large shifts of the electron and hole quasi-Fermi-levels, as photoexcited carriers become trapped in shallow states close to the mobility edges. Thus, the nonequilibrium occupancy of tail states can be studied easily by light-induced spin resonance (LESR), and such studies have already been performed.[40] However, these earlier studies have only focused on the LESR spectra of intrinsic paramagnetic states in compensated *a*-Si:H, which are due to holes in valence-band-tail states and electrons in the weak antibonding states of the conduction band tail. As shown in Fig. 22(a), the LESR resonance in compensated *a*-Si:H can be decomposed into the valence-band hole resonance at $g=2.011$ and the conduction-band electron resonance at $g=2.0044$. For comparison, the electron resonance of the conduction-band-tail line in singly phosphorus-doped *a*-Si:H is included, also [upper trace in Fig. 22(a)]. If we analyze the LESR spectra of compensated *a*-Si:H in Fig. 22(a) in terms of electron and hole concentrations, we find for compensation levels above 10^{-4} that the LESR density of trapped holes is always much larger than the density of trapped electrons. This is already obvious from the central trace in Fig. 22(a) where, a compensation level of $[PH_3]=[B_2H_6]=10^{-3}[SiH_4]$, the electron resonance at $g=2.0044$ is much smaller than the hole resonance at $g=2.011$. This asymmetry is even more pronounced for the optically detected magnetic resonance (ODMR) spectrum of the same sample shown in

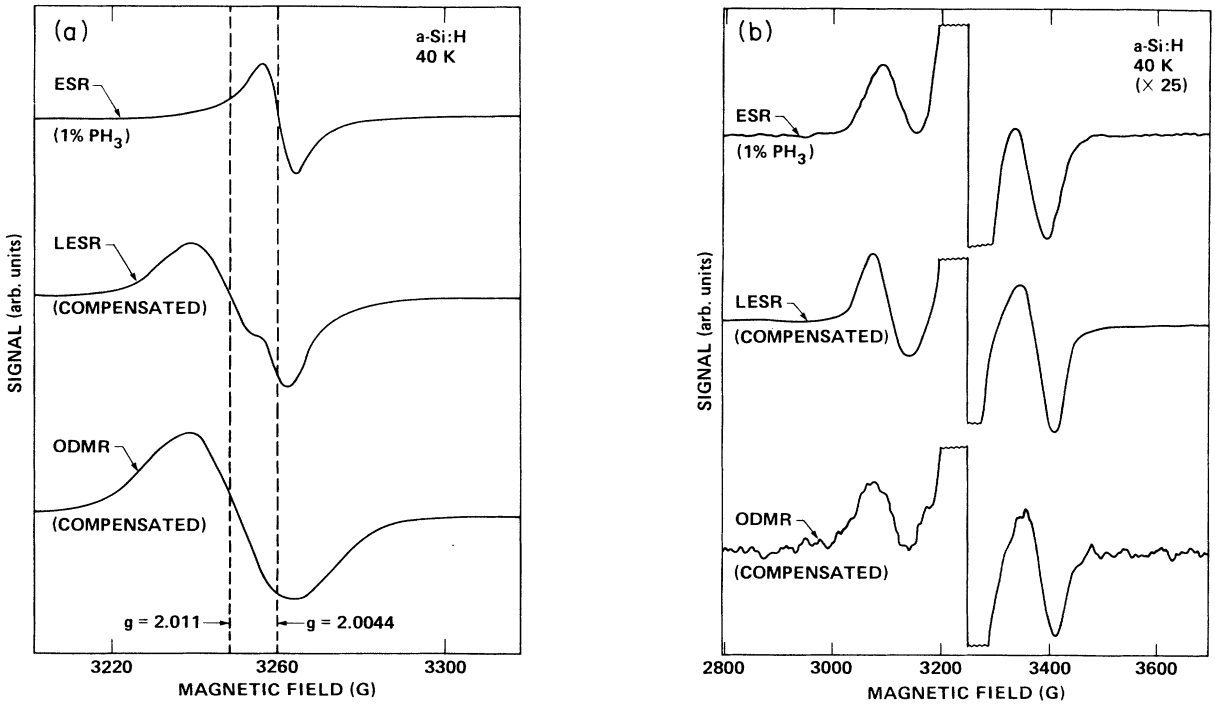

FIG. 22. ESR, light-induced ESR, and ODMR spectra of doped and compensated *a*-Si:H. (a) Central resonances due to electrons and holes in conduction- and valence-band tails. (b) Hyperfine spectra of electrons in neutral donor levels. Note the change in scale between (a) and (b).

the lower curve. Since ODMR experiments measure the influence of paramagnetic states on the radiative transitions (luminescence) in a sample,[79] we can conclude that there is a large difference between the role of holes in valence-band-tail states and the role of electrons in conduction-band-tail states as far as trapping and recombination processes in compensated *a*-Si:H are concerned.

On the other hand, the charge neutrality condition in compensated material requires that the densities of electrons and holes in shallow traps measured by LESR should be equal. To the extent that these traps are tail states, our previous results have shown that they are mostly singly occupied and paramagnetic (cf. Fig. 3). Therefore, in order to explain the electron-hole asymmetry of the LESR (and ODMR) spectra in Fig. 22(a), we have to assume that electron traps other than conduction-band-tail states ($g=2.0044$) are present in compensated materials. Indeed, the extended and magnified LESR and ODMR spectra in Fig. 22(b) show that the phosphorus donor levels themselves are actively involved in the trapping and recombination process. The characteristic hyperfine structure of P_4^0 states is clearly resolved, and the hyperfine spectrum of singly phosphorus-doped *a*-Si:H is again shown for comparison. For a more quantitative discussion, in Fig. 23 the electron and hole densities in the various trap states calculated from the low-temperature LESR spectra are summarized. VB, CB, and hf refer to holes in valence-band-tail states, electrons in conduction-band-tail states, and electrons in neutral donor states, respectively. In undoped *a*-Si:H, all optically excited electrons and holes are trapped in tail states, leading to nearly equal intensities of the VB and CB resonances ($\approx 10^{17}$ cm^{-3} at $T=40$ K and for a light intensity of 160 mW/cm^2). As the compensation level of the material is increased from zero to 3×10^{-3}, no changes in the density of holes trapped in valence-band-tail states is observed. On the other hand, the LESR density of electrons trapped in conduction-band-tail states decreases rapidly with compensation level, from 10^{17} cm^{-3} in undoped material to $\approx 10^{14}$ cm^{-3} for a 3×10^{-3} compensation. At the same time, however, the density of electrons in neutral donor states increases in such a way as to keep the total density of trapped electrons constant at a level of 10^{17} cm^{-3}, thereby fulfilling the charge neutrality requirement:

$$N(\mathrm{VB})=N(\mathrm{CB})+N(\mathrm{hf})\approx 10^{17}\ \mathrm{cm}^{-3}\ . \tag{22}$$

Thus, for compensation levels larger than 10^{-4} we can conclude from the LESR measurements that the nature of the predominant electron traps changes quite abruptly from conduction-band-tail states to neutral donor levels, whereas the holes are always trapped in shallow valence-band-tail states, independent of the compensation. In addition, since the trapped electrons and holes are the initial and final states for the radiative transitions observed in ODMR, the same picture provides a natural explanation for the form of the ODMR spectra, namely a superposition of the valence-band tail and neutral donor resonances

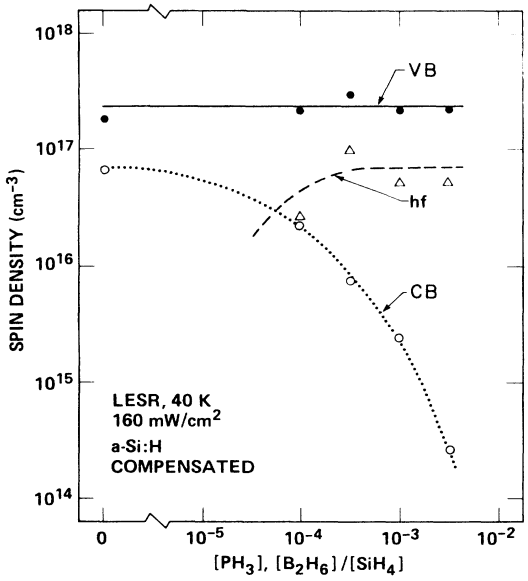

FIG. 23. Dependence of the LESR spin densities in compensated a-Si:H on compensation level. VB, CB, and hf refer to holes in valence-band-tail states, electrons in conduction-band-tail states, and electrons in neutral donor levels, respectively.

[see Figs. 22(a) and 22(b)].

From the relative intensities of the conduction-band tail and the neutral donor resonances in Fig. 23 one can attempt to estimate the donor density of states as a function of compensation level. To this end, we assume that the electron capture cross sections for both types of traps are not largely different, and also that the conduction-band-tail density of states to first order is unaffected by the compensation. With these assumptions, the occupancy of tail states and donor levels by electrons during a LESR experiment can be described by the same electron quasi-Fermi-level $E_{F,n}$, and the LESR density of tail states ($g=2.0044$) can be used as a common reference for the various compensation levels. In other words, the ratio of electrons trapped at neutral donor sites and electrons trapped in conduction-band-tail states provides a measure for the ratio of the corresponding densities of states at $E_{F,n}$. The experimental data in Fig. 23 thus suggest that $N_D(E_{F,n})\approx N_{\rm CB}(E_{F,n})$ for a compensation level of 10^{-4}, whereas $N_D(E_{F,n})\approx 10^3 N_{\rm CB}(E_{F,n})$ at a 10^{-2} compensation level. For a correct interpretation of these results, however, it is also necessary to know the dependence of the quasi-Fermi-level position on the compensation. This information can be obtained by measuring the magnitude of the hyperfine splitting, ΔH, for the neutral donor LESR signal as a function of compensation level. According to Eqs. (20) and (21), ΔH is expected to depend on the energy depth $\Delta E=E_c-E_{F,n}$ of the neutral donors seen in the LESR spectra as

$$\Delta H = C\,|\,E_c - E_{F,n}\,|^{3/2}\,. \tag{23}$$

With ΔH measured in gauss and ΔE in meV, an approximate value for the proportionality constant is $C\approx 0.1$. Experimental values for ΔH at various compensation levels are shown in Fig. 24, together with the corresponding splitting in singly phosphorus-doped material. The hyperfine splitting of the LESR resonances in compensated a-Si:H is generally larger than the 245 G splitting in phosphorus-doped samples. At the highest compensation levels, a value of $\Delta H=285$ G is obtained. Using Eq. (23), we can calculate the corresponding shift of $E_c-E_{F,n}$ to be about 15 meV, from 150 meV at low compensation to approximately 165 meV at a 1% compensation level. Therefore, we think it likely that the behavior of the LESR electron densities in Fig. 23 is not due to a shift of the average donor energies (and consequently of $E_{F,n}$) to lower energies, but instead reflects a strong increase of the ratio $N_D/N_{\rm CB}$ near E_c-150 meV with compensation due to an increase of the concentration of active donors. If we scale our density-of-states model for singly phosphorus-doped material in Fig. 14 accordingly, we can estimate the density of active dopants in a-Si:H with a compensation level of 1% to be approximately 10^{20} cm^{-3}. This means that the doping efficiency in compensated a-Si:H for a 1% doping level is about 2 orders of magnitude larger than the doping efficiency for the case of single doping. We will discuss this interesting result in more detail in Sec. IV.

The experimental data in Figs. 22 and 23 show quite conclusively that the trapping and radiative recombination process in compensated a-Si:H are largely influenced by the donor levels (P_4^+, P_4^0). This distinguishes compensated from undoped samples, where only the "intrinsic" conduction- and valence-band-tail states appear in the ODMR and LESR spectra. The fact that the hyperfine-split donor sites constitute the majority of the electron trapping centers in compensated a-Si:H with phosphorus and boron levels above 100 ppm has other interesting influences on the behavior of this material. As a first example we would like to mention the effect of the changed

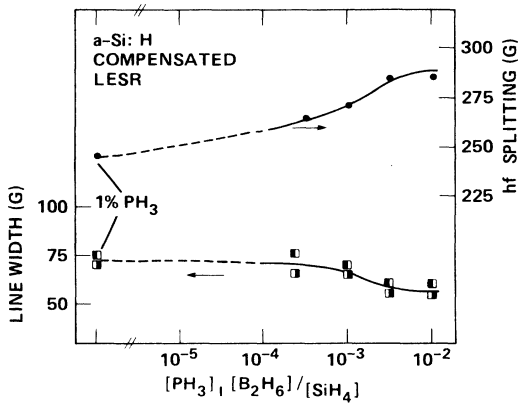

FIG. 24. Variation of the peak-to-peak linewidth and the hyperfine splitting of the ^{31}P LESR spectra in compensated a-Si:H with compensation level. Data for a 1% singly phosphorus-doped sample is shown for comparison. Left- and right-shaded symbols refer to the low- and high-field hyperfine line.

character of the major electron trap on the light-induced degradation of *a*-Si:H. This degradation is believed to occur by breaking of weak Si—Si bonds into two metastable dangling bonds in the course of nonradiative recombination between photoexcited electrons and holes. In undoped *a*-Si:H, the electrons and holes are trapped in antibonding and bonding orbitals of weak bonds, constituting the conduction- and valence-band tails, respectively. If, for a given electron-hole pair, the spatial overlap of the wave functions of both carriers is sufficiently large (i.e., both carriers are trapped effectively in two orbitals of the same or adjacent weak bonds), a nonradiative transition can become possible, whereby the electronic excitation energy is locally transformed into vibrational energy. This, then, can provide the local structure excitation necessary for the breaking of the weak bond. (For more details on light-induced changes in *a*-Si:H, see Refs. 80—82 and references therein.) In the present context, the important point is that the microscopic process leading to the light-induced degradation of undoped *a*-Si:H requires a spatial correlation between photoexcited electrons and holes. Now, in compensated *a*-Si:H this spatial correlation is destroyed, since, as shown above, photogenerated electrons are predominantly trapped at donor sites, whereas holes are still trapped by bonding orbitals of weak bonds. If the proposed microscopic model for the creation of light-induced dangling bonds is correct, one has to expect, therefore, that the degradation observed in compensated *a*-Si:H decreases as the fraction of photoelectrons trapped in donor states increases with compensation level. This is, indeed, the case. In Fig. 21, the open circles indicate the measured dangling-bond density after light degradation. Note the excellent agreement between the data in Fig. 21 and the electron trapping behavior in Fig. 23.

A second interesting aspect of electronic excitations in compensated *a*-Si:H is shown in Fig. 25. There, we have compiled LESR and ODMR hyperfine spectra of *a*-Si:H with a relatively high compensation level (1% PH_3 and B_2H_6 in a deposition plasma). The interesting feature is the appearance of an additional pair of hyperfine lines with a magnetic field splitting of $\Delta H = 125$ G, indicated by the arrows in Fig. 25. The LESR spectrum shows that the steady-state density of the corresponding spin states is relatively small $\approx 10^{14}$ cm^{-3} compared to a total density of trapped electrons and holes of about 10^{17} cm^{-3}. Nevertheless, these states dominate the ODMR hyperfine structure, as can be seen in the two lower traces in Fig. 25. The ODMR spectra contain both the outer ($\Delta H \approx 250$ G) and inner ($\Delta H \approx 125$ G) pairs of hyperfine lines also seen in LESR, but the resonant changes of the luminescence signal associated with the inner hyperfine lines dominate, especially for small phase shifts, ϕ, between the magnetic field modulation and the phase-sensitive detection of the resonant luminescence changes.

Further information about the electronic processes responsible for the LESR and ODMR spectra in Fig. 25 can be obtained from time-resolved ODMR measurements. Figure 26 shows the transient responses of the luminescence in compensated *a*-Si:H at $T = 40$ K, when a resonant microwave field is turned on and off. The three different traces are obtained by satisfying the magnetic

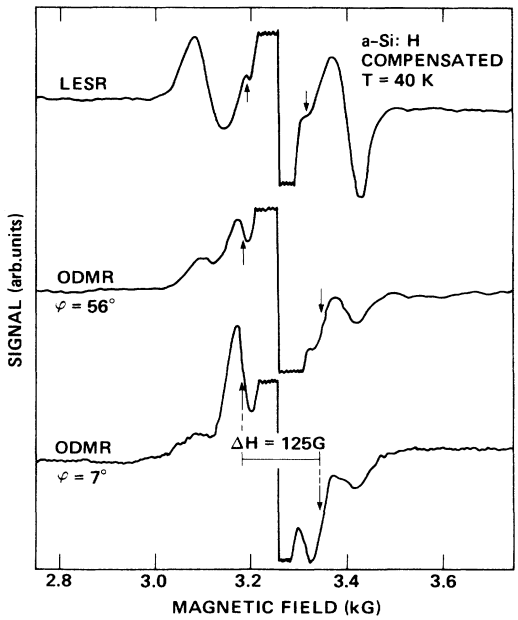

FIG. 25. Light-induced electron-spin-resonance (LESR) and optically detected magnetic resonance (ODMR) spectra of compensated *a*-Si:H ($[PH_3]=[B_2H_6]=10^{-2}[SiH_4]$, $T=40$ K). Arrows indicate the hyperfine spectrum due to donor-bound electron-hole pairs with a field splitting of $\Delta H = 125$ G. The angle φ in the ODMR spectra denotes the phase shift between the magnetic field modulation and the lock-in detector for the luminescence signal.

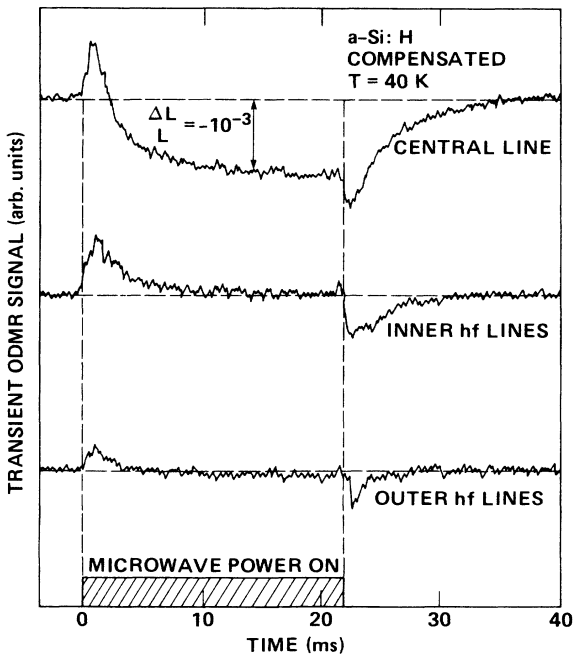

FIG. 26. Time-resolved ODMR transients of the sample in Fig. 25. The traces show the resonance luminescence signal $\Delta L/L$ for the central resonance, the inner hyperfine lines ($\Delta H = 125$ G), and the outer hyperfine pair ($\Delta H = 250$ G) in Fig. 25.

resonance conditions for the central ODMR line, the inner pair of hyperfine lines, and the outer pair of hyperfine lines. Positive going transients indicate a resonant enhancement of the luminescence intensity, L ($\Delta L > 0$). These transients suggest that the electronic states corresponding to the inner hyperfine lines are involved purely in a radiative, luminescent transition, the probability of which is enhanced by spin resonance. A similar conclusion holds for the outer pair of hyperfine lines, only that in this case the resonant enhancement is less pronounced. Note that this is consistent with the LESR spectrum in Fig. 25, which indicates that the electronic states causing the outer lines have a longer lifetime (and, therefore, a higher steady-state concentration in LESR) than the states connected with the inner lines, which appear to exhibit a faster radiative decay. On the other hand, the central ODMR resonance has both, enhancing character at short times and a pronounced quenching character at longer delay times. This behavior suggests that the electronic states underlying the central resonance also takes part in a nonradiative recombination transition, thus causing a decrease of the compensating luminescent transition upon spin resonance.

B. Discussion

Although there are many interesting aspects concerning the magnetic resonance response (LESR and ODMR) of compensated a-Si:H itself, in the following discussion we will focus our attention more on those issues relevant to the doping process and dopant states in a-Si:H.

Figure 27 is a schematic model for the electronic density of states in compensated a-Si:H as it can be deduced from the ESR and LESR measurements. As indicated by the solid and dashed curves in this figure, the density of states can be divided into two contributions: (i) states intrinsic to a-Si:H, which are also present in undoped material (solid), and (ii) states introduced by the dopants (dashed curves). The ESR results presented in Sec. II B suggest that the density of intrinsic electronic states remains fairly unchanged by the compensation. Specifically, there is no compensation-induced enhancement of dangling-bond defects, as demonstrated e.g., by the ESR results shown in Fig. 21, and also by optical measurements.[74] Consequently, most of the differences between compensated and undoped a-Si:H must be due to the dopant-related states. To be more specific, if we consider the case of a-Si:H compensated with B and P, the relevant states are B_3^0, B_4^-, B_4^0, P_3^0, P_4^+, and P_4^0. In addition, we have to allow for a certain degree of direct donor-acceptor bonding, leading for example to the formation of $(Si)_i$—B—P—$(Si)_j$ complexes ($i,j=2,3$). Recent NMR double-resonance experiments have shown that for a compensation level of 1%, about half of the dopant atoms actually are incorporated in the form of such complexes.[83] However, it is likely that most of these dopant-related states do not have a significant influence on the observed electronic processes in compensated a-Si:H. This has already been discussed in the case of the nondoping threefold-coordinated configurations, B_3^0 and P_3^0. In a similar way, one can argue that B—P complexes, too, are not electronically active in a-Si:H. The reason lies in the larger bonding-antibonding splitting for a B—P bond compared to Si—Si bonds.[84] This means that electronic states related to the B-P pairs probably will not lie in the mobility gap of a-Si:H.

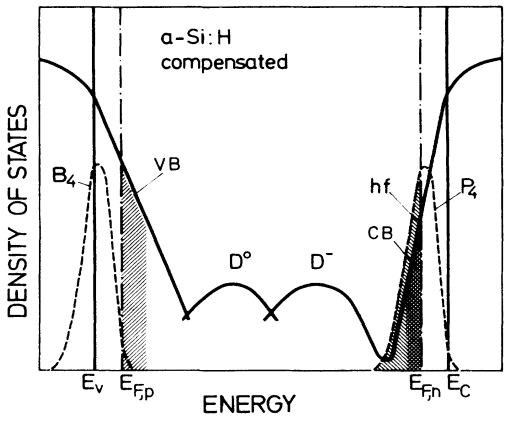

FIG. 27. Schematic model for the density of states in compensated a-Si:H. Valence-band tail, dangling bonds, and conduction-band tail are denoted by VB, D^0 and D^-, and CB, respectively. P_4 and B_4 refer to the bands of active donors and acceptors. The electron and hole quasi-Fermi-level positions, $E_{F,n}$ and $E_{F,p}$, under illumination at low temperatures are indicated by dashed-dotted lines. Hatched regions show the electronic states contributing to the LESR signal. hf is the fraction of neutral donor states responsible for the hyperfine-split spin resonance signal.

These preliminary ideas are further supported by the present ESR and LESR measurements. As demonstrated by the spectra in Fig. 22, the only paramagnetic states observed in a-Si:H either in thermal equilibrium or under illumination at low temperatures are as follows: neutral dangling bonds, Si_3^0; holes trapped in weak Si—Si bonding states, $(Si_4\text{-}Si_4)^+$; electrons trapped in weak Si—Si antibonding states, $(Si_4\text{-}Si_4)^-$; electrons trapped at donor sites, P_4^0, As_4^0. The important point is that these states not only are all the paramagnetic defects observed, but also account for all states required by charge neutrality, even under illumination and for varying doping levels (cf. Fig. 23). For the case of compensated a-Si:H, this fact allows the conclusion that if there are any other dopant-related defects in the gap of a-Si:H than those listed above, their density has to be negligible so as not to disturb the charge neutrality in the samples.

On the other hand, the density-of-states model in Fig. 27 can account for most experimental observations. The density of dangling-bond defects is low and independent of the compensation level. This is demonstrated by the constant density of neutral dangling bonds observed in ESR (Fig. 21) as well as by the high and compensation-level-independent density of photoexcited carriers observed in LESR (Fig. 23). The same LESR measurements demonstrate that the character of the valence-band-tail states remains fairly unchanged by the compensation. In all compensated samples studied, hole trapping was al-

ways due to weak Si—Si bonds ($g \approx 2.011$). This shows at the same time that the active acceptors necessary for the compensation of the large density of active donors must have electronic levels quite far into the valence-band tail, so as to make them unobservable in LESR. In Fig. 27, this is indicated by an acceptor density of states (B_4 peak) below the hole quasi-Fermi-level $E_{F,p}$. Quite differently, conduction-band-tail states and phosphorus donor levels occur in the same energy range and are both intersected by the electron quasi-Fermi-level $E_{F,n}$, emphasizing their role as electron traps. Depending on the compensation level, either conduction-band-tail states or donor states will be more abundant, thereby dominating the electron trapping. Roughly equal densities of active donors and tail states are obtained for a gas-phase doping level of $[B_2H_6]/[SiH_4]=[PH_3]/[SiH_4]\approx 10^{-4}$. A comparison of the ratio of conduction-band-tail states and donor levels as a function of compensation level has allowed us to conclude that the doping efficiency for both acceptors and donors in compensated a-Si:H is much higher than for the case of single doping (e.g., $\approx 10\%$ versus 0.1% for a dopant concentration of 1%).

The observation of the donor hyperfine spectra in LESR and ODMR allows further conclusions concerning the microscopic configuration of these states. We have already mentioned above that the similar P_4^0-hyperfine splitting seen in compensated a-Si:H and singly doped material suggests roughly identical donor wave functions in both cases. For example, it is quite unlikely that the majority of the active donors in compensated a-Si:H occur in the form of B_4^--P_4^+ pairs, since the interaction with a charged boron atom with its significant nuclear magnetic moment should have noticeable effects on the hyperfine splitting of an electron trapped at the phosphorus site.

Another remarkable feature in the magnetic resonance spectra of compensated a-Si:H is the appearance of an additional pair of hyperfine lines with a splitting of $\Delta H \simeq 125$ G, half of the hyperfine splitting observed for the neutral donors in the same material. A likely explanation for these resonances are exchange-coupled electron-hole pairs located at the site of an active phosphorus donor. (In a way, such a state could be called a donor bound exciton in compensated a-Si:H, consisting of an electron localized at the site of a P_4 atom and coupled to a hole trapped in an adjacent weak Si—Si bond via exchange interaction.) The paramagnetic state thus can be pictured as the $S=1$ triple state formed by exchange interaction between a neutral donor electron ($\Delta H=250$ G) and a hole trapped in a nearby weak-bonding orbital ($\Delta H=0$). Indeed, this would provide a straightforward explanation for the observed hyperfine splitting of $\Delta H \approx 125$ G. Note also that similar conclusions have been reached in low defect density, undoped a-Si:H based on the analysis of the g value of ODMR spectra.[79] In the latter case, the resonance was identified via its g value, which was observed as the arithmetic average between that of electrons in conduction-band-tail states ($g=2.0044$) and of holes in valence-band-tail states ($g=2.011$). In addition, all other experimental observations support the identification of the $\Delta H=125$ G hyperfine pair in compensated a-Si:H with exchange-coupled electron-hole pairs close to a donor site. For example, this resonance is only observed at the highest compensation levels ($\leqq 3\times 10^{-3}$), hence demonstrating the involvement of the donor states. Also, exchange-coupled states are likely to have short radiative lifetimes, which explains the dominating role of the corresponding resonances in the ODMR spectra as well as the low steady-state concentrations observed in the LESR spectra.

Finally, some comments concerning the new ESR results described in Sec. III B in relation to earlier investigations of carrier trapping and recombination in compensated a-Si:H (Sec. III A) should be made. The main difference between these earlier investigations and the present study is the direct observation of the P_4 states and the implications already discussed above. For electrons in compensated a-Si:H the presence of these states results in an increase of the average trap depth, in qualitative agreement with the luminescence and transport experiments cited in Sec. III A. Quantitatively, however, there are quite severe differences. According to the present LESR measurements, the average trap depth of electrons increases only by about 20 meV, whereas the corresponding increase estimated from transport measurements is about 1 order of magnitude larger [≈ 300 meV (Ref. 17)]. A similar situation is observed for the case of holes trapped in the valence-band tail of compensated a-Si:H. The LESR spectra indicate no significant changes in the hole trapping behavior (only small changes in the LESR line shape occur), whereas hole mobility measurements again suggest an increase of the average hole trap depth by roughly 300 meV.[77] The results of the mobility measurements are also consistent with the observed decrease of the luminescence peak energy in compensated a-Si:H by about 0.4 eV.[40]

At present, we can only speculate on possible reasons for these quantitative differences. An important point one has to keep in mind is that different experimental techniques (time-of-flight, luminescence, LESR) generally observe different properties of the charge carriers trapped in compensated a-Si:H during illumination. For example, the LESR response is dominated by carriers with the longest (nonradiative and radiative) lifetimes and provides information about the microscopic environment of these carriers in their trapped state. Luminescence, on the other hand, will be dominated by those carriers with short radiative lifetimes. Hence, LESR and luminescence can lead to different conclusions, to the extent that different subsets of trapped excited carriers are observed. An example for this difference is given by the exchange-coupled electron-hole pairs described above: The contribution of these states to the LESR response of compensated a-Si:H is negligible, whereas under identical conditions the resonant luminescence response is strongly influenced by the existence of these pairs (cf. Fig. 25).

As far as mobility measurements are concerned, further complications can be expected from the fact that the time-of-flight experiments used for the determination of the carrier drift mobility observe carrier transport over macroscopic distances in the material under investigation. Differences between conclusions derived from such mac-

roscopic experiments and from microscopic techniques such as LESR, then, are unavoidable if the samples studied exhibit inhomogeneities on a length scale which will leave the microscopic technique unaffected, but will strongly disturb any macroscopic transport experiment. In compensated *a*-Si:H, likely candidates for such long-scale inhomogeneities are potential fluctuations caused by the presence of large densities of charged dopants (B_4^-, P_4^+). An interesting question for future investigations will be to resolve some of these discrepancies between different experimental techniques in the case of compensated amorphous silicon.

IV. DOPING MODELS

So far, we have mostly discussed the influence of doping on the electronic density of states in hydrogenated amorphous silicon and germanium. In the remainder of this article we will address the questions of how the dopant atoms responsible for these changes are incorporated into the solid films and what mechanisms are likely to determine the doping efficiencies, i.e., the fraction of the incorporated atoms which are electronically active.

A. Thin-film deposition and dopant incorporation

The first step in the doping process is the incorporation of the dopant atoms into the amorphous *a*-Si:H or *a*-Ge:H network. Here we have to discern between dopant incorporation occurring during or after the actual deposition of the amorphous film. Post-deposition doping techniques are doping via ion implantation[85,86] or neutron transmutation.[87] Both methods require additional heat treatments to anneal out radiation damage, and are less effective than codeposition doping. The latter technique makes use of the fact that the presence of gases like phosphine (PH_3), arsine (AsH_3), or diborane (B_2H_6) during the deposition process leads to an incorporation of P, As, or B in the growing thin film. However, whereas the solid-phase concentration of the dopant atoms can easily be calculated for post-deposition doping, in the case of codeposition doping the incorporation efficiency is found to depend quite strongly on the specific deposition conditions and also on the different dopant gases. A careful analysis of the atomic composition of the doped material as a function of the dopant gas concentration is, therefore, always necessary.

Thin films of *a*-Si:H or *a*-Ge:H have been successfully deposited by a large number of deposition techniques, which make use of glow-discharge or chemical vapor deposition of silane (SiH_4) and germane (GeH_4), or sputtering from solid Si and Ge in a hydrogen atmosphere.[88] Deposition is made with a predetermined mixture of reactive gases, characterized by the volume concentration of dopant gases, i.e., PH_3, AsH_3, or B_2H_6, in the main gases, SiH_4 or GeH_4. This gas-phase (or plasma) concentration will in the following be denoted by C_{gas}. Often, the mixture of reactive gases is further diluted in more or less "inert" carrier gases like Ar, Ne, He, or H_2. The gas has to be excited in order to overcome the potential barrier against the hydrogen loss reactions leading to the formation of the solid phase (e.g., $n\mathrm{SiH_4} \rightarrow n\mathrm{Si_{sol}} + 2n\mathrm{H_2}\uparrow$). Excitation may occur by raising the temperature of the gas until a spontaneous equilibrium chemical vapor deposition (CVD) sets in,[89–92] by physically exciting the gas through resonant absorption of light (Hg photosensitation,[93] CO_2-laser-assisted deposition[94]), or by exciting a plasma in a sufficiently strong rf or dc electric field. Plasma deposition allows one to vary the deposition conditions from those characteristic for physical vapor deposition (PVD: high power density, strongly diluted reactive gases, heavy ion bombardment, far from thermal equilibrium) to deposition conditions approaching the CVD limit (low-power rf-glow discharge, undiluted reactive gases, floating substrate potential). The latter conditions are the ones most commonly used today for the deposition of state-of-the-art *a*-Si:H (doped or undoped), and the essentially CVD character of the deposition has been demonstrated recently.[95] Doping of amorphous silicon and germanium has also been achieved using the rf-sputtering technique.[96]

The atomic concentration of dopant atoms in the solid phase, C_{sol}, can be determined using a variety of different techniques. These methods comprise nuclear activation of dopant atoms,[97] secondary-ion mass spectrometry,[90] or, at higher dopant concentrations, Auger electron spectroscopy and electron microprobe analysis.[98] In Fig. 28 some published results for C_{sol} versus C_{gas} in *a*-Si:H doped with P, As, or B have been compiled for a number of different deposition techniques. It is quite evident that for a given dopant concentration in the gas mixture used for the deposition, the concentration of dopant atoms actually incorporated into the solid film can vary by many orders of magnitude, depending on the deposition conditions, and also on the nature of the reactive gases. Because of our lack of understanding of the processes occurring during the deposition of amorphous Si and Ge, it is impossible to account for the experimental data in Fig. 28 in any detail. Nevertheless, some general remarks seem appropriate.

Two limiting cases are evident from Fig. 28. All experimental points seem to be located between the two dashed lines, which are given by the relations $C_{sol} = C_{gas}$ (linear incorporation) and $C_{sol} = (C_{gas})^{1/2}$. Secondly, for any given gas mixture, the $C_{sol} = C_{gas}$ limit is obtained for deposition conditions favoring physical vapor deposition (PVD), whereas the $C_{sol} = (C_{gas})^{1/2}$ limit is approached for deposition conditions closer to a chemical reaction in thermal equilibrium (CVD). For example, deposition through an energetic (dc) glow discharge at low temperatures and with considerable dilution in inert gases almost invariably leads to a linear incorporation of the dopants, independent of their nature (As, P, or B). The reason is quite clear: The large and homogeneous supply with energy masks any differences in the chemical reactivity of the various molecules and radicals present in the gas phase. As a consequence, the composition of the growing solid film just mirrors the partial pressures of the various gases in the plasma. On the other hand, if the energy input per molecule is just sufficient to activate the hydrogen-loss reactions necessary for the formation of the solid phase, the

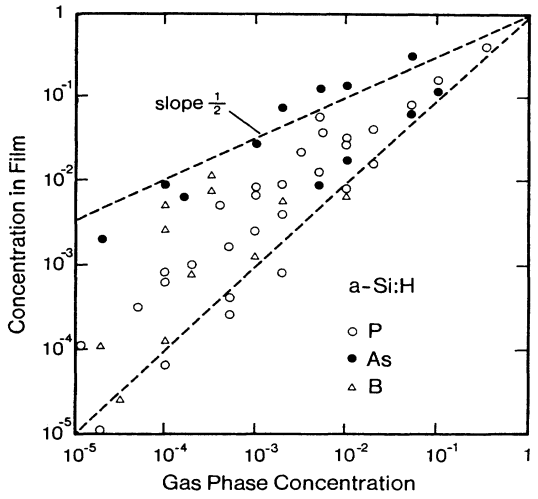

FIG. 28. Incorporation probability for P, As, and B into hydrogenated amorphous silicon prepared by various deposition techniques. Shown is the dependence of the dopant concentration in the solid film on the dopant-gas concentration in the deposition gas mixture. Dashed lines indicate the limits of linear and square-root incorporation.

deposition rate of the various species will be determined by a thermal equilibrium between the participating products and educts. Then the incorporation of dopants will be governed by a system of coupled chemical reactions depending on chemical reaction energies and the relative concentrations of dopants in both the gaseous and the solid phase. Under these conditions, a departure from a linear incorporation of dopants into the host matrix can occur. Indeed, deposition processes operating close to thermal equilibrium conditions (e.g., low-power, rf-glow discharge of undiluted gases, high-temperature depositions) generally lead to a deviation from the PVD limit, $C_{\rm sol}=C_{\rm gas}$, and tend to be close to the second limiting relation in Fig. 28, i.e., $C_{\rm sol}=(C_{\rm gas})^{1/2}$. Note that such a "square-root" dependence is generally to be expected for a chemical reaction of the type

$$AB \rightleftarrows A+B\ . \tag{24}$$

Then, because of $[A]=[B]$, the law-of-mass action yields

$$\frac{[A][B]}{[AB]}=\frac{[A]^2}{[AB]}=\frac{[B]^2}{[AB]}=\text{const} \tag{25a}$$

or

$$[A]=[B]\propto[AB]^{1/2}\ , \tag{25b}$$

where we have denoted the concentrations of the species involved in the reaction (24) by square brackets.

Even for a fixed deposition method the concentration of dopants in a given host matrix depends strongly on the dopant-host system. This is illustrated in Fig. 29 for the glow-discharge (GD) technique. The solid-phase concentrations of P, As, and B are shown for doped GD a-Si:H and a-Ge:H as a function of the corresponding gas-phase concentrations. Again, it is quite clear that the exponent s in the relation $C_{\rm sol}\propto C_{\rm gas}^{s}$ can take any value between $s\approx 0.5$ and $s\approx 1$ for the different dopant-host systems, corresponding to the CVD and PVD limits discussed above. For a-Ge:H, $s=0.5$ is seen for P doping, whereas $s=1.1$ in B-doped material. In a-Si:H, $s=0.6$ is observed in As-doped samples, and $s=0.8$ describes both P- and B-doped a-Si:H.

Some insight into the data of Fig. 29 can be found from a related deposition method, Hg-sensitized photo-CVD (Ref. 93 and references therein). This method is quite similar to a low-power rf-plasma deposition in that the process has CVD rather than PVD character,[93,95] and the activation of these chemical processes occurs through

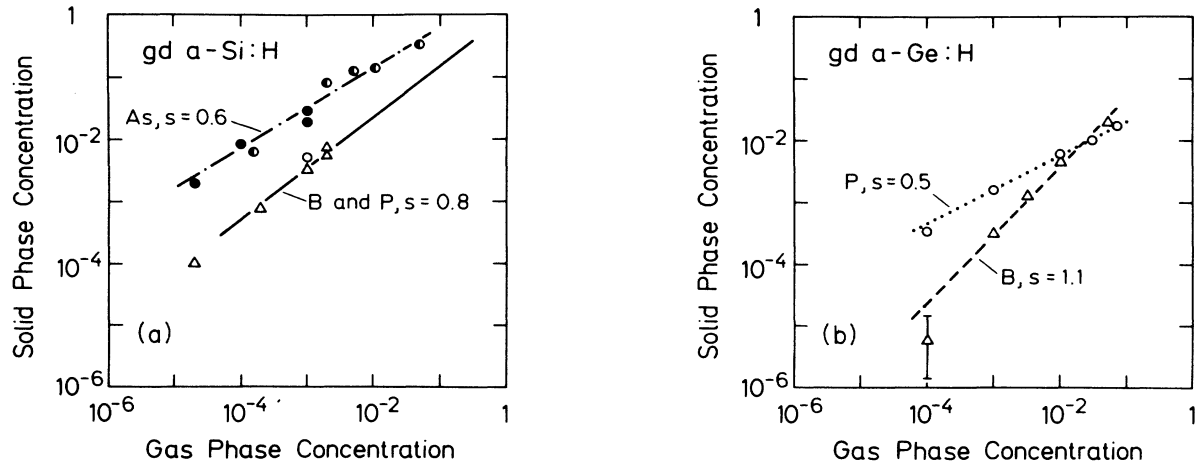

FIG. 29. Dopant incorporation probability for hydrogenated amorphous silicon (a) and germanium (b) prepared by the glow-discharge techniques. s denotes the exponent in the relation $C_{\rm sol}-C_{\rm gas}^{s}$, where $C_{\rm sol}$ ($C_{\rm gas}$) is the chemical concentration (partial pressure) of the doping species in the deposited solid film (deposition plasma).

electronic excitation. In the case of Hg-sensitized photo-CVD, this excitation is provided via resonant absorption of light emitted from a mercury lamp by Hg atoms mixed with the gases to be deposited. From an analytical point of view, the advantage of this method is that the amount of (activation) energy transferred into a specific gas, and therefore the probability of the chemical reactions limiting the solid-phase deposition can be measured quite accurately.[99] Typically, the results of these measurements are expressed in terms of a quenching cross section for the resonant Hg radiation ($\lambda=2537$ and 1849 Å). Values for the gases of interest here are listed in Table VIII.

Although the relevance of these cross sections for rf-glow-discharge processes may be questioned, they are in surprisingly good agreement with a number of observations made in rf plasmas. For example, the ratio of the cross sections for silane and germane according to Table VIII is 1:5.4. This has to be compared with the relative incorporation rates for Si and Ge in rf plasma deposited *a*-SiGe alloys, which have been measured is 1:5 up to 1:7.[100] Or, the incorporation of nitrogen into SiN alloys deposited from NH_3-SiH_4 plasmas should be suppressed by a factor of about 8, again in quite good agreement with the experimental observations.[101] As far as the incorporation of dopants into *a*-Si:H is concerned, the values in Table VIII suggest that As should be strongly enriched in *a*-Si:H, whereas P should be incorporated with a 1:1 probability. Moreover, for the same gas-phase concentrations, all dopants should be approximately 5 times more concentrated in *a*-Si:H than in *a*-Ge:H. All this is in good qualitative agreement with the data in Fig. 29.

We next address the strongly sublinear dependence of the solid-phase concentration on the gas-phase concentration observed for As in *a*-Si:H and P in *a*-Ge:H. As pointed out before, such a behavior can result from a situation in which the rate-limiting step for the dopant incorporation is governed by a bimolecular chemical reaction [Eq. (24)]. It is, therefore, quite interesting to note that the As—As (P—P) bond strength is significantly larger than the As—H (P—H) bond strength, whereas for Ge, Si, and B the bonding to hydrogen has a similar or even larger strength than bonding between like atoms (Table IV, Ref. 61). This, then, would promote the formation of molecules containing As_2 (P_2) units in sufficiently dense AsH_3 (PH_3) plasmas. If the incorporation of these molecules into a growing *a*-Si:H or *a*-Ge:H film is inhibited relative to the incorporation of molecules or radicals containing only one As (P) atom, a square-root dependence of the solid state on the gas-phase concentration can result. A similar situation actually exists for the preparation of phosphorus-doped crystalline silicon from thermal CVD of SiH_4-PH_3 gas,[102] and the reader is referred to this work for further details.

TABLE VIII. Quenching cross sections for chemical vapor deposition of various gases (Ref. 93).

Gas	Photo-CVD cross section (Å^2)
SiH_4	26
GeH_4	140
PH_3	26
AsH_3	very large
B_2H_6	unknown
NH_3	3
H_2	6

B. The doping efficiency

Before we can attempt a discussion of the possible doping mechanisms in amorphous silicon or germanium, we have to obtain an experimental determination of the number of active dopants in a given sample. Since active and inactive dopant atoms can be expected to differ by their coordination number (four versus three), early experiments were designed to observe this difference directly. The first experiment of this kind was performed by Knights *et al.*, who used extended x-ray-absorption fine structure (EXAFS) measurements to investigate doping of *a*-Si:H with arsenic.[103] As a result of these measurements, the authors concluded that for a solid-phase As concentration of about 4×10^{20} cm^{-3} approximately 20% of the arsenic atoms are fourfold coordinated. This would mean that of the order of 10^{20} cm^{-3} donor electrons are present in a 1% As-doped *a*-Si:H sample. If we compare this number with the concentration of excess electrons in glow-discharge *a*-Si:H doped with As shown in Figs. 19 and 20, we note that the result obtained from the EXAFS measurements is too high by at least an order of magnitude. The probable reason for this discrepancy has to do with the fact that the way hydrogen bonds to As and Si atoms in *a*-Si_xAs_{1-x}:H will have a large influence on the average coordination of these atoms as measured by EXAFS, because the presence of hydrogen cannot be detected by this method. For example, there has been experimental evidence for preferential bonding of hydrogen to arsenic,[104] as well as for strong changes in the hydrogen bonding environment with changing arsenic concentration.[66] In view of these large uncertainties in the reduction of the EXAFS data, we believe that an accurate determination of the doping efficiency in *a*-Si:H for the interesting range of dopant concentrations (≤ 1 at. %) is not feasible. In the case of the more common dopants in *a*-Si:H, phosphorus and boron, EXAFS measurements cannot be used because of the small x-ray contrast of the dopant atoms relative to the *a*-Si:H matrix. Therefore, nuclear magnetic resonance of the ^{31}P and ^{11}B nuclei has been used for an investigation of the coordination of these dopants in *a*-Si:H.[105–107]

It appears that a direct structural determination of the doping efficiency in *a*-Si:H or *a*-Ge:H is quite difficult and can be complicated by clustering of dopant atoms or bonding to hydrogen. Especially the latter aspect of doping in *a*-Si:H can be quite important, in view of the recent discovery of dopant passivation by hydrogen in crystalline semiconductors.[108–110] A more meaningful and reliable estimate of the doping efficiency in the amorphous semiconductors can be obtained by determining the concentration of excess charge carriers in the doped relative to undoped material, quite in analogy to crystalline semicon-

ductors. In the amorphous materials, however, the measurement of the excess charge concentration is complicated by the fact that excess carriers can be trapped by the amphoteric dangling-bond defects near midgap to form Si_3^+ or Si_3^- states and, moreover, by the experimental observation that the density of these defects changes with doping level (see Sec. II D). Hence, in order to measure the excess charge introduced by electronically active dopants, one has to determine not only the concentration of electrons or holes in shallow states (tail states and neutral dopants, see Fig. 20), but also the concentrations of dangling-bond defects in their various charge states. Here, we can address this problem by combining the electron-spin-resonance measurements shown in Figs. 2(a) and 2(b) with the optical-absorption data summarized in Fig. 19. The optical-absorption measurements yield the total dangling-bond density, $N=N^+ + N^0 + N^-$, fairly independent of the relative charge states, since these different states have roughly identical cross sections for optical transitions out of or into extended states. On the other hand, the ESR spin density only probes the density N^0, of neutral, singly occupied dangling bonds. Depending on the dangling-bond density in the undoped case, two situations can occur. In *a*-Si:H, the density of neutral dangling bonds, N^0, is usually less than or equal to 10^{16} cm^{-3} for the various doping levels [Fig. 2(a)]. In contrast, the optical-absorption measurements show that the total dangling-bond density N is significantly larger than N^0 for doping levels above 10^{-5}. This indicates that in doped *a*-Si:H nearly all dangling bonds have been charged by trapping a dopant electron or hole. Since, in addition, the density of carriers in shallow states is always much smaller than the density of charged dangling bonds, to a good approximation the number of electronically active dopants in this material is given just by the number of charged dangling-bond defects measured by optical methods (luminescence, absorption, LESR). This fact can be employed to determine the doping efficiency in high-quality *a*-Si:H only from optical data.[111]

In *a*-Ge:H, however, this approach is not correct, since the total dangling-bond density N, as shown in Fig. 19, is always quite similar to the ESR spin density of neutral dangling bonds in undoped samples, $N^0 \approx 8\times 10^{17}$ cm^{-3} [Fig. 2(b)], at least for doping levels up to 10^{-3}. Hence, in order to calculate the doping efficiency in *a*-Ge:H, not only the total dangling-bond density N from optical measurements has to be known, but also the fraction N^0 of ESR-active neutral dangling bonds. Only then the density N_{act} of active dopants can be determined:

$$N_{act}=N-N^0+n \tag{26}$$

(n denotes the density of charge carriers in shallow states, see Fig. 20). In Eq. (26) we have made use of the fact that $N^+ \ll N^-$ ($N^- \ll N^+$) for n-type (P-type) samples. In terms of this equation, the difference between *a*-Si:H and *a*-Ge:H is that in *a*-Si:H, $N \gg n - N^0$ for all doping levels above 10 ppm, whereas a similar approximation in *a*-Ge:H is only valid for doping levels exceeding 10^3 ppm.

In any case, with the experimental data for N^0, N, and n already shown in Figs. 2(a), 2(b), 19, and 20, it is now easy to calculate the density of active dopants, N_{act}, and, thus, the doping efficiency using Eq. (26). However, according to our remarks above, we are faced with the yet unsolved problem of what dopant concentrations we should relate the calculated values of N_{act} to in order to obtain a meaningful doping efficiency η. Two extreme viewpoints seem possible.[112] The first possibility is to define a solid-phase doping efficiency η_{sol} as the ratio of the density of active doptans to the total concentration of dopant atoms in the solid amorphous film N_{sol}:

$$\eta_{sol}=\frac{N_{act}}{N_{sol}} . \tag{27}$$

This definition assumes implicitly that all dopant atoms incorporated into the solid are, in principle, capable of forming active dopant sites. In other words, Eq. (27) is a reasonable definition of the doping efficiency in *a*-Ge:H and *a*-Si:H, if most constraints imposed by the solid phase determine whether an incorporated dopant atom is electronically active or not. The experimental values for the solid-phase doping efficiency η_{sol} are compiled in Fig. 30 for the various dopant-host systems investigated. For the calculation of η_{sol} we have made use of the incorporation data in Figs. 29(a) and 29(b). As a general observation, η_{sol} decreases from about 10% for low dopant concentrations to about 0.1% at the highest doping levels and is therefore by about 2 orders of magnitude smaller than estimated from the direct structural investigations described above. The scatter between the solid-phase doping efficiencies for the different dopant-host systems is about a factor of 10. More important, the dependence of η_{sol} on the dopant concentration is qualitatively different: P in *a*-Ge:H and As in *a*-Si:H show a doping efficiency η_{sol} which is nearly independent of the dopant concentration in the solid phase, whereas the other dopant-host pairs exhibit a sublinear decrease of η_{sol} with increasing dopant concentration.

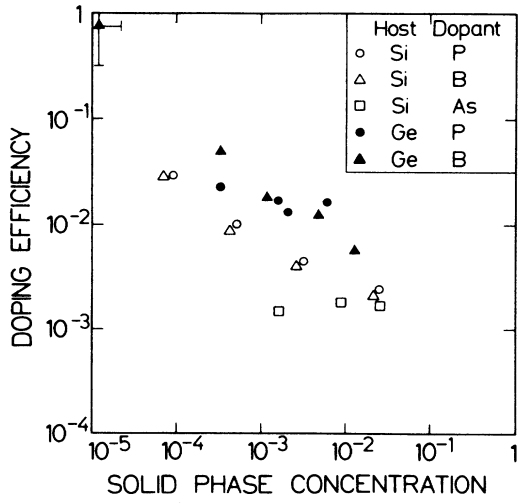

FIG. 30. Solid-phase doping efficiency [see Eq. (27)] as a function of solid-phase dopant concentration for glow-discharge *a*-Si:H and *a*-Ge:H samples doped with P, As, or B.

A second possibility for the definition of the doping efficiency in a-Si:H and a-Ge:H is obtained by relating the density N_{act} of active donors in the deposited solid film to the gas-phase concentration N_{gas} of dopant atoms present in the deposition plasma (for example, $N_{gas}=[PH_3]/[SiH_4]$ in the case of phosphorus-doped a-Si:H). The resulting "total doping efficiency,"

$$\eta_{tot}=\frac{N_{act}}{N_{gas}} \tag{28}$$

can be regarded as the product of the solid-phase doping efficiency η_{sol} and the dopant incorporation efficiency η_{inc}:

$$\eta_{tot}=\frac{N_{act}}{N_{gas}}=\left[\frac{N_{act}}{N_{sol}}\right]\left[\frac{N_{sol}}{N_{gas}}\right]=\eta_{sol}\eta_{inc}\ . \tag{29}$$

The definition of a doping efficiency according to Eq. (28) is reasonable if we assume that the concentration of active dopants after deposition is limited by reactions in the plasma used for the deposition. Such a situation will occur, for example, if an active solid-phase dopant requires a certain precursor in the deposition plasma for its formation, and can be quite important for the deposition technique used for high-quality a-Si:H or a-Ge:H, namely rapid solidification from a low-energy plasma. Experimental results for the total doping efficiency η_{tot} in a-Ge:H and a-Si:H are summarized in Fig. 31. In comparison to Fig. 30 it should be noted that the second definition of the doping efficiency [Eq. (28)] leads to a common, unique behavior for all five dopant-host pairs, namely an efficiency which decreases like a square root with increasing dopant gas concentration and, moreover, agrees within a factor of 2 for all dopants in a-Si:H and a-Ge:H. Obviously, for this to happen, Eq. (29) requires that variations in the incorporation efficiency (η_{inc}) and the solid-phase doping efficiency (η_{sol}) cancel exactly over 4 orders of magnitude in the doping gas concentration and for all dopants in a-Si:H and a-Ge:H. This remarkable result suggest that the creation of active dopants in these materials is closely related to the plasma chemistry such that the same reactions enabling an enhanced incorporation probability for the two cases of P in a-Ge:H and As in a-Si:H have no similar influence on the formation of active dopant sites. Or, in other words, the gas-phase species responsible for the enhanced incorporation do not lead to the formation of active dopant sites.

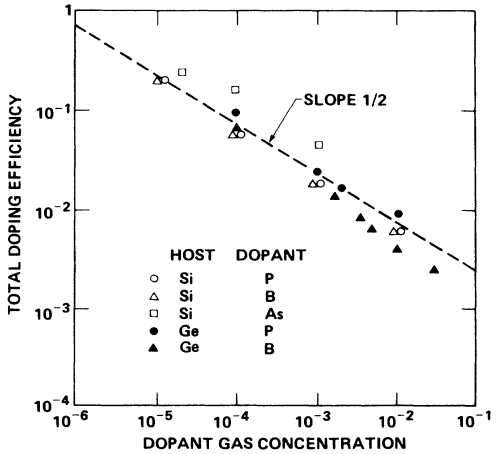

FIG. 31. Total doping efficiency [see Eq. (28)], as a function of dopant gas concentration in the deposition plasma for the samples in Fig. 30.

C. Doping models

There have been several attempts to develop qualitative and semiquantitative models for the doping process in a-Si:H. In order to account for the experimental results presented in this paper, a realistic doping model should be capable of explaining consistently the following points.

(i) The doping efficiency in a-Si:H and a-Ge:H is much lower than in the corresponding crystalline materials and generally tends to decrease with increasing dopant concentrations (either in the deposited film or in the gas mixture used for deposition).

(ii) The majority of the excess electrons or holes introduced by doping does not occupy shallow tail states, but rather deep dangling-bond defects, whose concentration increases with increasing doping level (autocompensation, doping-induced dangling bonds).

(iii) In contrast, compensated samples have a constant, low density of dangling-bond defects, despite a greatly enhanced doping efficiency.

(iv) The incorporation of dopant atoms into an amorphous film depends strongly on the specific deposition process used. For chemical vapor depositionlike processes, strong enrichment of dopants is quite common. However, increased incorporation does not cause an increased doping efficiency. This means that dopant atoms which are incorporated preferentially, on the average, end up in a nondoping configuration.

Originally, the absence of doping in amorphous semiconductors and, as a first approximation, the quite small doping efficiency in amorphous silicon and germanium was explained by Mott, who extended the well-known Octet rule for chemical molecular valences to the bonding situation in amorphous solids.[10] Mott's "$8-N$ rule" states that, because of the largely reduced topological constraints in an amorphous solid, every atom will bond with a coordination of $Z=\min(N, 8-N)$, where N is the number of valence electrons. Then, as discussed in the Introduction, doping will not occur.

However, the experimental observation of doping in a-Si:H showed that the $8-N$ rule cannot be applied uncritically to every amorphous semiconductor, but that modifications are necessary. Specifically for the case of a-Si:H, one of us (R.A.S.) proposed in 1982 that for a better description of the doping process the $8-N$ rule has to be extended so as to include charged configurations of the matrix atoms [111]. It was argued that, for example, a positively charged phosphorus atom (P^+) is isoelectronic to a neutral silicon atom (Si^0) and, as a consequence, will prefer a fourfold coordination, resulting in a P_4^+

state. Similarly, a negatively charged Si atom is isoelectronic to a neutral P atom, thus bonding preferentially as Si_3^- (threefold coordinated). This being the case, doping in *a*-Si:H can be understood, in the context of a "modified $8-N$ rule," as a valence alternation-charge exchange process:

$$Si_4^0 + P_3^0 \rightleftarrows Si_3^- + P_4^- , \tag{30}$$

where both sides obey the modified rule (including charged species), but the left-hand side describes a nondoping situation, whereas the right-hand side refers to an active dopant atom which has donated a carrier to a compensating, doping-induced dangling bond. Of course, similar arguments apply to the case of *p*-type doping, e.g., with boron. Doping in *a*-Si:H can then be modeled in terms of a "chemical equilibrium" between the two sides in Eq. (30), probably established during the deposition of the material, when the network is still flexible enough to allow the necessary valence alternation. The large success of this model is a consistent description of the doping efficiency in *a*-Si:H and of the creation of new dangling-bond defects by the doping process. More details are given in Refs. 75, 111, and 113. In addition, it was pointed out that the modified $8-N$ rule could be used to establish a more general connection between the Fermi- or quasi-Fermi-level position and the density of structural defects (dangling bonds) in a material like *a*-Si:H. According to the modified $8-N$ rule, the coordination of a matrix atom depends on the charge state of this atom, which in turn is determined by the Fermi-level position. Thus, the modified $8-N$ rule is not only capable of describing the basic aspects of doping in *a*-Si:H, but also other examples of charge-induced defect creation in this material. A more-detailed discussion of the various implications of the modified $8-N$ rule on the electronic properties of *a*-Si:H can be found in a recent article by Müller *et al.*[114] In addition, Robertson has discussed microscopic aspects of the $8-N$ rule relevant to doping in amorphous silicon.[115,116]

Despite the obvious success of Street's model in explaining the most salient features of doping in *a*-Si:H, closer inspection of the experimental results raises some doubts as to whether this model alone is sufficient to account in detail for the many facets of the process in question. For example, amorphous silicon and germanium can sustain quite large densities of electronic states which are forbidden by the $8-N$ or the modified $8-N$ rule. The most prominent example in undoped material is the neutral dangling bond, Si_3^0 or Ge_3^0. In doped *a*-Si:H and *a*-Ge:H, the observation of occupied tail states (CB or VB) and of neutral donor levels (P_4^0 and As_4^0) are further examples. The obvious reason for the occurrence of these states is that an amorphous network like *a*-Si:H is not totally free of structural constraints, so that this necessary condition for the applicability of the $8-N$ rule is not fulfilled. Important structural constraints present in amorphous silicon and germanium are the overcoordination of the tetrahedral network,[117] promoting the formation of strain-relieving dangling-bond defects, and the preservation of short-range order, which imposes certain constraints on the possible bonding configuration of nontetrahedral species like dopants. Recognizing this fact, the present authors have already pointed out possible modifications of the ideal $8-N$ rule in order to arrive at more realistic doping models.[118]

A second and rather important point is that the $8-N$ rule describes doping in *a*-Si:H and *a*-Ge:H only in terms of solid-phase species like Si_3, P_4, and so on. This, however, is a quite severe simplification of the actual situation in that possible memory effects in the solid phases are neglected. Remember that, generally, the preparation of amorphous silicon or germanium requires a rapid solidification of gas-phase or plasma precursors in order to prevent immediate crystallization of a sample. After all, the preparation of *a*-Si:H or *a*Ge:H is based on the fact that the solid phase or surface mobility of the deposited atoms is sufficiently low, preventing them from attaining their absolute minimum-energy configuration. Obviously, the same must be true for the dopant species. This picture implies that the assumption of a thermal equilibrium at the growing surface is incompatible with the formation of an amorphous Si or Ge network. This is also true for the probability of a dopant atom to become incorporated into the solid amorphous film on an electronically active or inactive site, and therefore the doping efficiency may well depend on what was the precursor of the atom in the deposition plasma and on subsequent reactions at the growing surface. As an implication, it would be very fortuitous if the doping efficiency in *a*-Si:H and *a*-Ge:H could be described by a chemical equilibrium between solid-state species allowed by the $8-N$ rule. Indeed, the experimental data for the doping efficiency shown in Figs. 30 and 31 suggest that the gas-phase dopant concentration rather than the solid-phase concentration determines the doping efficiency in *a*-Si:H and *a*-Ge:H, an experimental result which clearly cannot be understood in the context of the doping model based on the modified $8-N$ rule. In the case of phosphorus-doped *a*-Si:H, Kampas and Vanier have recognized this fact and have developed a doping model which explicitly includes gas-phase species.[119] However, their model is much too specialized to be able to account for the common dependence of the doping efficiency on the gas-phase dopant concentration shown in Fig. 31 for the five different dopant-host systems investigated here. In addition, the doping efficiency for a given dopant-host pair at a fixed dopant concentration can be expected to depend quite strongly on the deposition procedure employed if gas-phase reactions are important. Indeed, recent measurements on sputtered *a*-Si:H doped with As and B support this conjecture.[120]

To summarize the arguments given above, it is quite likely that gas-phase reactions and gas-surface interactions have an important if not dominating influence on the doping efficiency in glow-discharge-deposited *a*-Si:H and *a*-Ge:H. This result actually constitutes a step backwards in our understanding of the doping process, since it is not only necessary to take into account the various configurations of dopant atoms in the solid film, but also the complicated gas-phase chemistry leading to the incorporation of dopants. Moreover, different deposition techniques very likely require somewhat different models for the dopant incorporation and the doping efficiency. In the case of the low-power glow-discharge deposition tech-

nique, a rate-limiting step for the incorporation of active dopant atoms might be the loss of the third, unpaired hydrogen atom common to the usual dopant gases PH_3, AsH_3, or $(BH_3)_2$. More details concerning this point can be found in a separate publication.[121]

We conclude that the simple assumption of thermal equilibrium at the growing surface is unable to account for all the doping efficiency results, particularly the As-doping data. On the other hand, we do not have a general model for gas-phase reactions to explain the universal square-root dependence of η_{tot} on gas concentrations (Fig. 31) as well as the different dopant incorporation rates (N_{sol}/N_{gas}). The properties of compensated a-Si:H further confuse the picture. Our data show that the doping efficiency of compensated samples is very high compared to singly doped material. The original doping model readily accounts for this result because it is an expected consequence of the Fermi energy remaining in the middle of the band gap. However, to the extent that the dopant incorporation is a separate process governed by gas reactions, then this simple explanation can no longer apply.

If one assumes that the doping efficiency in a-Si:H and a-Ge:H is determined by the way dopant precursors are formed in the gas phase and are finally incorporated into the solid, a separate explanation has to be found for the doping-induced increase in the density of compensating dangling-bond defects. In particular, we can no longer expect that these dangling bonds are formed at the same time as the formation of an active dopant takes place, e.g., as described by Eq. (30). Indeed, there is some experimental evidence that dangling-bond formation and incorporation of active dopants are governed by distinct processes. One example is the case of lithium doping of a-Si:H.[122,123] Since Li forms an interstitial donor in a-Si:H, it will not affect directly the coordination of other network atoms. Nevertheless, the same doping-induced creation of deep dangling-bond defects has been observed in Li-doped a-Si:H.[124] This indicates quite clearly that the increase in the dangling-bond density upon doping is not a consequence of valence alternation between dopant and matrix atoms, but rather a secondary effect induced by the excess charge donated by the dopants. It appears, therefore, that not the incorporation of active dopants, but the resulting shift of the Fermi level is responsible for the creation of new dangling-bond defects. This notion is consistent with the experimental fact that, in a similar fashion, shifts of the quasi-Fermi-level induced by charge injection or illumination can induce excess dangling bonds,[81,125,126] even in undoped a-Si:H and after deposition.

In the case of undoped a-Si:H, the appearance of these dangling bonds was ascribed to the charge-induced breaking of weak Si—Si bonds, whose electronic levels form the tails of the valence and conduction bands. This situation, however, is Street's original argument for doped a-Si:H, based on the modified $8-N$ rule. According to this rule, the favorable coordination of a silicon atom will depend on the charge state of the atom, and therefore on the Fermi- or quasi-Fermi-level position. In the neutral charge state, the fourfold-coordinated configuration, Si_4^0, is energetically favorable. When, however, the (quasi-) Fermi level is shifted and a silicon atom becomes positively or negatively charged, a threefold-coordinated dangling-bond state, Si_3^+ or Si_3^-, will be preferred. In this context, it is not important whether the charging of a previously neutral Si atom is achieved by doping, illumination (carrier trapping), or charge injection. In any case, creation of new dangling bonds is the result, and the modified $8-N$ rule provides a consistent description of charge-induced structural changes in a-Si:H, at least on a phenomenological level.

Microscopically, on the other hand, this charge-induced dangling-bond creation is somewhat more difficult to perceive. A restriction imposed on possible microscopical models may be that the bond breaking necessary for the creation of new Si-dangling bonds could require strong charge localization, and thus involves a process which is restricted to a small number of matrix atoms. For extended states, electronic wave functions are so delocalized that the effective charge of any given atom in the solid film is not appreciably altered, even by the introduction of 10^{19} cm^{-3} excess charge carriers via doping or injection.

For a-Si:H, electronic levels which have to be considered in a modified $8-N$ scheme as discussed above are shown schematically in Fig. 32. States close to or above either mobility edge are not likely to be involved (see also the results in Fig. 15). This leaves the hatched regions of the band tails, namely states ≈ 0.2 eV below E_C, which are of weak antibonding character, and the weak-bonding-like valence-band-tail states 0.3—0.4 eV above E_V. In addition, the deep, strongly localized nonbonding dangling-bond states with an effective correlation energy of $\approx +0.3$ eV will be important. We will now show that many instances of charge-induced dangling-bond creation

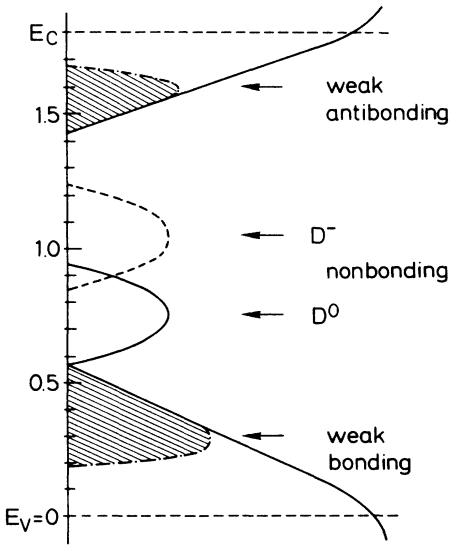

FIG. 32. Schematic model for the density of electronic states in a-Si:H involved in charge-induced weak-bond—dangling-bond conversion. Energies are given in eV relative to the valence-band mobility edge E_V. See text for further details.

in a-Si:H, particularly doping, can be explained by considering only the states shown in Fig. 32.

The model is based on the charge-induced conversion between the bonding and antibonding orbitals of a weak Si—Si bond, and two nonbonding sp^3 orbitals (dangling bonds) created by structural relaxation (bond breaking). In the weak bond configuration, the overlap between the two sp^3 hybrid orbitals is sufficient to produce bonding and antibonding molecular orbitals close to normal band states, i.e., in the hatched regions of Fig. 32. In the neutral charge state of the two-atom cluster, only the bonding orbital near E_V will be occupied by two electrons. When excess electrons or holes are introduced by charge injection or doping, these carriers can be trapped in the localized orbitals of the cluster and can lead to bond breaking. The necessary relaxation could involve an increase of the distance between the two Si atoms, changes of the bond angle by rotation (increasing the π bonding character), and dangling-bond switching by local hydrogen movement (see also Ref. 81). This conversion of a weak bond into two dangling bonds, therefore, removes one molecular orbital from each of the hatched regions in Fig. 32, and adds two new sp^3 hybrids (dangling bonds) near midgap. As a consequence the change in electronic energy occurring with the structural relaxation will depend quite strongly on the charge state of the cluster during the conversion. To see this, consider, for example, the neutral state, where each atomic hybrid contributes one electron. In the weak bond configuration, these two electrons will occupy the bonding orbitals with a total electronic energy relative to E_V of $\approx 2\times 0.3$ eV. In the dangling-bond configuration, the same two electrons must remain in the nonbonding D^0 orbitals near midgap, so that their energy would be $\approx 2\times 0.8$ eV. Obviously, in this neutral charge state, bond breaking is energetically unfavorable. The situation is different, however, in the twice negatively charged state, when the orbitals of the cluster are occupied by four electrons. In the weak-bond state, again two electrons occupy the bonding orbital, but in addition the antibonding orbital is also doubly occupied. This gives an electronic energy of $\approx 2\times 0.3$ eV $+ 2\times 1.6$ eV $= 3.8$ eV. In the dangling-bond configuration, on the other hand, all four electrons are in atomic sp^3 orbitals, each of which carries a single negative charge (D^-). Because of the stronger localization of these orbitals, electronic correlation effects, which could be neglected for the more delocalized tail states, have to be taken into account, raising the energy of each doubly occupied sp^3 hybrid by the effective dangling-bond correlation energy, $U_{\text{eff}} \approx 0.3$ eV. Thus, the total electronic energy in the dangling-bond configuration is $\approx 4\times 0.8$ eV $+ 2\times 0.3$ eV $= 3.8$ eV. Similar estimates can be made for all possible charge states of the cluster, and the results are summarized in Table IX. This table shows that the charge-induced creation of dangling bonds is energetically possible especially in the two double charge states $2+$ and $2-$. Physically, this makes sense, because only for these charges the number of bonding and antibonding electrons are equal (0 in the $2+$ state, 2 in the $2-$ state), thus promoting bond breaking. In addition, the presence of two charges leads to a Coulomb repulsion which can further help to increase the spatial separation between the two sp^3-hybrid orbitals. Note also, that such a microscopic mechanism is consistent with the modified $8-N$ rule discussed above. Since the formation of dangling bonds by bond breaking topologically requires simultaneous changes of the coordination of two atoms, two charges are also necessary to induce these changes.

A more-detailed discussion of this model and an extension to other situations of dangling-bond creation in a-Si:H can be found elsewhere.[127] Here, we will only discuss some implications for the doping process in a-Si:H and a-Ge:H. The microscopic process of the weak-bond—dangling-bond conversion allows us to explain the phenomenon of doping-induced dangling-bond defects independent of the formation of active dopant sites. This is in better agreement with our experimental results concerning the doping efficiency in a-Si:H and a-Ge:H than for earlier doping models. In the present model, given a certain density of active dopants (or excess charges introduced by a different means), conversion of intrinsically present weak bonds into dangling bonds will take place as long as any doubly charged tail states remain, since these states are unstable according to Table IX and the $8-N$ rule. Thus, the model provides an explanation for the lacking correlation between the doping efficiency and the dangling-bond density in general (cf. Figs. 19 and 31), and especially for the fact that mostly singly occupied, paramagnetic shallow states are observed in a-Si:H (see Fig. 3). In addition, the existence of such states, which would have been forbidden by the modified $8-N$ rule as originally proposed, is explained consistently by the present model.

V. SUMMARY AND CONCLUSIONS

In this study, we have explored substitutional doping in hydrogenated amorphous silicon and germanium. In order to obtain a sufficiently large data base, five different dopant-host systems have been investigated, employing the same experimental techniques (electron-spin-resonance and related methods, optical absorption, transport measurements, and chemical composition analysis) in each case. Based solely on combined ESR and transport measurements, models for the electronic density of states of a-Si:H and a-Ge:H can be deduced, which are in good

TABLE IX. Electronic energies relative to E_V for the weak-bond and the dangling-bond configuration of two Si sp^3 hybrids as a function of the charge state. ΔE is the energy difference between the two configurations. See text for further explanation.

	Electronic energy (eV)		
Charge	Weak bond	Dangling bond	ΔE
0	0.6	1.5	0.9
+	0.3	0.8	0.5
	2.2	2.7	0.5
2+	0	0	0
2−	3.8	3.8	0

agreement with the results of other experimental methods. Based on these models, differences between the responses of *a*-Ge:H and *a*-Si:H to *n*- and *p*-type doping can be understood.

In the cases of doping with phosphorus and arsenic, a characteristic hyperfine structure due to the interaction of donor electrons with the dopant nuclei is observed in the ESR spectra. A detailed analysis of these spectra can be used to obtain a microscopic model for the underlying donor wave functions. It is shown that the various donor states in *a*-Ge:H and *a*-Si:H are well described by *s*-like wave functions with effective Bohr radii between 9 and 11 Å. Together with recent hyperfine investigations for Si dangling bonds, this allows us to quantitatively describe the energy dependence of the localization length in the mobility gap of *a*-Si:H.

In order to obtain a quantitative model for the density of states near the conduction-band mobility edge E_C in doped samples, the dependence of the ESR spectra in *n*-type *a*-Si:H and *a*-Ge:H on doping level and temperature has been investigated. Combined with optical-absorption measurements of doping-induced changes in the density of deep dangling-bond levels, these results are used to deduce the energetic distribution of P and As donor levels. It is found that phosphorus forms a donor band approximately 100 meV below E_C, with a full width at half maximum of 120 meV in both *a*-Si:H and *a*-Ge:H. Arsenic in *a*-Si:H forms a similar donor band, but shifted to lower energies by about 50 meV.

As far as deep dangling-bond-defect levels are concerned, a comparison of optical subgap absorption results shows marked differences between the response of this defect density to doping for the various dopants and hosts. Whereas the dangling-bond density in doped *a*-Ge:H is, to first order, independent of the doping level, *a*-Si:H samples exhibit a pronounced increase of the dangling-bond density. By comparing dangling-bond densities in doped *a*-Si:H and *a*-Ge:H with the total density of shallow levels (tail states and neutral dopants), it is found that for any given doping level, about 90% of the excess charge carriers introduced by the doping are trapped in compensating dangling-bond defects. The remaining 10% of shallow carriers are localized mostly in singly occupied, paramagnetic states.

In addition to singly doped material, compensated *a*-Si:H has been investigated with ESR, LESR, and ODMR methods as a function of compensation level. Based on these measurements it can be concluded that the electronically active states in this material are neutral dangling bonds, conduction- and valence-band-tail states, and neutral donor levels. Increasing the level of compensation leaves the dangling-bond density and the density of valence-band-tail states fairly constant, whereas the density of states in the conduction-band tail is dominated by donor states for compensation levels above 10^{-4}. This change in the nature of the dominant electron trap can be used to explain the smaller susceptibility of compensated *a*-Si:H to light-induced metastable dangling-bond creation. From the LESR results it is further concluded that the boron acceptor levels lie within a much larger density of valence-band-tail states and are, therefore, not directly involved in the trapping and recombination processes in compensated *a*-Si:H. At the highest compensation levels, the formation of donor bound exciton states is reported.

For a better understanding of the doping process in *a*-Si:H and *a*-Ge:H, the incorporation of dopant atoms from the deposition gas phase into the solid amorphous film have been investigated using secondary-ion-mass spectroscopy (SIMS) and electron microprobe measurements. Generally, it is observed that the concentration of dopant atoms in the solid phase for a given gas-phase concentration can vary by up to 2 orders of magnitude, depending on the gases involved and the nature of the deposition process. For glow-discharge-deposited *a*-Si:H and *a*-Ge:H, preferential dopant incorporation and strongly sublinear dependences between solid- and gas-phase concentrations are found in the cases of arsenic-doped *a*-Si:H and phosphorus-doped *a*-Ge:H. As a possible explanation for the latter observation, formation of As_2 and P_2 molecular species in the gas phases are discussed. By relating the density of electronically active dopants to the total concentration of dopant atoms in the solid film or in the deposition gas phase, two definitions for a doping efficiency in *a*-Si:H and *a*-Ge:H are obtained. Our results suggest that the gas-phase dopant concentration determines the doping efficiency in the deposited solid. For all five dopant-host pairs, a common decrease of the doping efficiency as the square root of the gas-phase concentration is observed, whereas no such correlation can be obtained with the solid-phase concentration.

Two models for doping in *a*-Si:H and *a*-Ge:H are discussed. The solid-phase equilibration model supposes that the creation of dangling-bond defects by doping is necessary for formation of active dopant sites, whereas in the chemical reaction equilibration model, dangling-bond creation is a secondary outcome of network rearrangement driven by the doping-induced charges.

ACKNOWLEDGMENTS

The authors would like to thank C. C. Tsai, R. Thompson, and A. J. Smith for sample preparation, and W. B. Jackson, N. M. Johnson, J. B. Boyce, and M. Rice for experimental support and many helpful discussions. This work was supported by the Solar Energy Research Institute (Golden, CO).

[1] *Hydrogenated Amorphous Silicon,* edited by J. I. Pankove (Academic, New York, 1984), Vol. 21A–21D.

[2] M. H. Brodsky and R. S. Title, Phys. Rev. Lett. **23**, 581 (1969).

[3] D. Kaplan, D. Lépine, Y. Petroff, and P. Thirry, Phys. Rev. Lett. **35**, 1376 (1975).

[4] W. E. Spear and H. L. Steemers, J. Non-Cryst. Solids **66**, 163 (1984).

[5] R. A. Street, J. Zesch, and M. J. Thompson, Appl. Phys. Lett.

43, 672 (1983).
[6]W. E. Spear and P. G. LeComber, Solid State Commun. **17**, 1193 (1975).
[7]C. Moss and J. F. Graczyk, Phys. Rev. Lett. **23**, 1167 (1969).
[8]R. J. Temkin, W. Paul, and G. A. N. Connell, Adv. Phys. **22**, 581 (1973).
[9]R. Mosseri, D. P. DiVincenzo, J. F. Sadoc, and M. H. Brodsky, Phys. Rev. B **32**, 3974 (1985).
[10]N. F. Mott, Adv. Phys. **16**, 49 (1967).
[11]R. A. Street and J. C. Zesch, Philos. Mag. B **50**, L19 (1984).
[12]W. B. Jackson, N. M. Amer, A. C. Boccara, and D. Fournier, Appl. Opt. **20**, 1333 (1981).
[13]W. E. Spear and P. G. LeComber, Philos. Mag. **33**, 935 (1976).
[14]W. E. Spear, Adv. Phys. **26**, 811 (1977).
[15]W. Beyer and H. Overhof, Solid State Commun. **31**, 1 (1979).
[16]H. Fritzsche, Solid Energy Mater. **3**, 447 (1980).
[17]D. Hauschildt, M. Stutzmann, J. Stuke, and H. Dersch, Solid Energy Mater. **8**, 319 (1982).
[18]J. Stuke, Philos. Mag. B **52**, 225 (1985).
[19]W. Beyer and H. Overhof, in *Semiconductors and Semimetals,* edited by J. I. Pankove (Academic, New York, 1984), Vol. 21C, p. 257.
[20]J. Hubbard, Proc. R. Soc. London, Ser. A **240**, 539 (1957).
[21]T. A. Kaplan, S. D. Mahanti, and W. M. Hartmann, Phys. Rev. Lett. **27**, 1796 (1971).
[22]H. Fukuyama and K. Yosida, J. Phys. Soc. Jpn. **46**, 1522 (1979).
[23]D. Adler and E. J. Yoffa, Phys. Rev. Lett. **36**, 1197 (1975).
[24]E. J. Yoffa and D. Adler, Phys. Rev. B **12**, 2260 (1975).
[25]H. Okamoto and Y. Hamakawa, Solid State Commun. **24**, 23 (1977).
[26]L. Schweitzer, M. Grunewald, and H. Dersch, Solid State Commun. **39**, 355 (1981).
[27]H. Dersch, J. Stuke, and J. Beichler, Phys. Status Solidi B **105**, 265 (1981). The value for the dangling-bond correlation energy of 0.4 eV in *a*-Si:H as given in this reference is too large because the doping-induced increase of the dangling-bond density (cf. Sec. II D) had not been taken into account. If this is done, one obtains a somewhat smaller value of $U_{\text{eff}} \approx 0.25$ eV.
[28]H. Dersch, J. Stuke, and J. Beichler, Phys. Status Solidi B **107**, 307 (1981).
[29]W. B. Jackson, Solid State Commun. **44**, 477 (1982).
[30]M. Stutzmann, J. Stuke, and H. Dersch, Phys. Status Solidi B **115**, 141 (1983).
[31]M. Stutzmann and J. Stuke, Solid State Commun. **47**, 635 (1983).
[32]M. Stutzmann and J. Stuke, Phys. Status Solidi B **120**, 225 (1983).
[33]Z. Vardeny and J. Tauc, Phys. Rev. Lett. **54**, 1844 (1985).
[34]H. Okamoto, H. Kida, T. Kamada, and Y. Hamakawa, Philos. Mag. B **52**, 1115 (1985).
[35]F. Schauer and J. Kocka, Philos. Mag. B **52**, L25 (1985).
[36]R. A. Street, D. K. Biegelsen, W. B. Jackson, N. M. Johnson, and M. Stutzmann, Philos. Mag. B **52**, 235 (1985).
[37]D. Adler, J. Phys. (Paris) Colloq. **42**, C4-3 (1981).
[38]Y. Bar-Yam and J. D. Joannopoulos, J. Non-Cryst. Solids **77-78**, 99 (1985).
[39]S. Hasegawa, T. Kasajima, and T. Shimizu, Philos. Mag. B **43**, 149 (1981).
[40]R. A. Street, D. K. Biegelsen, and J. C. Knights, Phys. Rev. B **24**, 969 (1981).
[41]J. C. Knights, D. K. Biegelsen, and I. Solomon, Solid State Commun. **22**, 133 (1977).
[42]A. Friedrich and D. Kaplan, J. Electron. Mater. **8**, 79 (1979).
[43]D. V. Lang, J. D. Cohen, and J. P. Harbison, Phys. Rev. B **25**, 5285 (1982).
[44]I. Solomon, R. Benferhat, and H. Tran-Quoc, Phys. Rev. B **30**, 3422 (1984).
[45]H. Fritzsche, J. Non-Cryst. Solids **77-78**, 273 (1985).
[46]T. Tiedje and A. Rose, Solid State Commun. **37**, 49 (1981).
[47]J. D. Cohen, J. P. Harbison, and K. W. Wecht, Phys. Rev. Lett. **48**, 109 (1982).
[48]W. Kohn, in *Solid State Physics,* edited by F. Seitz and D. Turnbull (Academic, New York, 1957), Vol. 5, p. 257.
[49]E. Fermi, Z. Phys. **60**, 320 (1930).
[50]M. Stutzmann and R. A. Street, Phys. Rev. Lett. **54**, 1836 (1985).
[51]C. C. Tsai, J. C. Knights, and M. J. Thompson, J. Non-Cryst. Solids **66**, 45 (1984).
[52]B. C. Fletcher, W. A. Yager, G. L. Pearson, A. N. Holden, W. T. Read, and F. R. Merritt, Phys. Rev. **94**, 1392 (1954).
[53]G. Feher, Phys. Rev. **114**, 1219 (1959).
[54]G. Feher, D. K. Wilson, E. A. Gere, Phys. Rev. Lett. **3**, 25 (1959).
[55]D. K. Wilson, Phys. Rev. A **134**, 265 (1964).
[56]G. S. Jackel and W. Gordy, Phys. Rev. **176**, 443 (1968).
[57]W. G. Zijlstra, J. M. Henrichs, J. H. M. Mooy, and J. D. W. van Voorst, Chem. Phys. Lett. **7**, 553 (1970).
[58]B. V. Shanabrook, S. G. Bishop, and P. C. Taylor, J. Phys. (Paris) Colloq. **42**, C4-865 (1981).
[59]P. C. Taylor, E. J. Friebele, and S. G. Bishop, Solid State Commun. **28**, 248 (1978).
[60]W. A. Harrison, Phys. Rev. B **24**, 5835 (1981).
[61]*CRC Handbook of Chemistry and Physics,* 60th ed., edited by R. C. West (The Chemical Rubber Co., Cleveland, OH, 1980), p. F-233ff.
[62]J. Robertson, Phys. Rev. B **28**, 4642 (1983); **28**, 4658 (1983); **28**, 4666 (1983).
[63]R. A. Street and D. K. Biegelsen, in *The Physics of Hydrogenated Amorphous Silicon,* edited by J. D. Joannopoulos and G. Lucovsky (Springer, Berlin, 1984).
[64]J. C. Knights, Philos. Mag. **34**, 663 (1976).
[65]Z. S. Jan, R. H. Bube, and J. C. Knights, J. Electron. Mater. **8**, 47 (1979).
[66]R. J. Nemanich and J. C. Knights, J. Non-Cryst. Solids **35/36**, 243 (1980).
[67]M. Stutzmann and D. K. Biegelsen, Phys. Rev. B **28**, 6256 (1983).
[68]J. R. Morton, Chem. Revs. **64**, 453 (1964).
[69]D. K. Biegelsen and M. Stutzmann, Phys. Rev. B **33**, 3006 (1986).
[70]N. Ishii, M. Kumeda, and T. Shimizu, Solid State Commun. **53**, 543 (1985).
[71]R. A. Street, in *Semiconductors and Semimetals,* edited by J. I. Pankove (Academic, New York, 1984), Vol. 21B.
[72]B. von Roedern, L. Ley, M. Cardona, and F. W. Smith, Philos. Mag. B **40**, 433 (1979).
[73]W. B. Jackson, S.-J. Oh, C. C. Tsai, and J. W. Allen, in *Optical Effects in Amorphous Semiconductors* (AIP Conf. Proc. No. 120), edited by P. C. Taylor and S. G. Bishop (AIP, New York, 1984), p. 341.
[74]W. B. Jackson and N. M. Amer, Phys. Rev. B **25**, 5559 (1982).
[75]R. A. Street, J. Non-Cryst. Solids **77/78**, 1 (1985).
[76]A. Skumanich and N. M. Amer, J. Non-Cryst. Solids **59/60**, 249 (1983).
[77]J. M. Marshall, R. A. Street, and M. J. Thompson, Phys. Rev. B **29**, 2331 (1984).

[78]C. Thomsen, H. Stoddart, T. Zhou, J. Tauc, and Z. Vardeny, Phys. Rev. B **33**, 4396 (1986).
[79]For a comprehensive treatment of ODMR in *a*-Si:H, see R. A. Street, Phys. Rev. B **26**, 3588 (1982).
[80]M. Stutzmann, W. B. Jackson, and C. C. Tsai, Appl. Phys. Lett. **45**, 1075 (1984).
[81]M. Stutzmann, W. B. Jackson, and C. C. Tsai, Phys. Rev. B **32**, 23 (1985).
[82]M. Stutzmann, W. B. Jackson, and C. C. Tsai, in *Materials Issues in Applications of Amorphous Silicon Technology,* Material Research Society Symposium Proceedings No. 49, edited by D. Adler, A. Madan, and M. J. Thompson (MRS, Pittsburgh, 1985), p. 301.
[83]S. Ready, J. B. Boyce, and C. C. Tsai, Bull. Amer. Phys. Soc. **31**, 236 (1986).
[84]See, e.g., *Bonds and Bands in Semiconductors,* by J. C. Phillips (Academic, New York, 1973), p. 42.
[85]S. Kalbitzer, G. Müller, P. G. LeComber, and W. E. Spear, Philos. Mag. B **41**, 439 (1980).
[86]G. Müller, H. Mannsperger, K. Böhringer, and S. Kalbitzer, in *Poly-, Microcrystalline, and Amorphous Semiconductors,* edited by P. Pinard and S. Kalbitzer (Les Éditions de Physique, Les Uils, 1984), p. 497.
[87]H. Hamanaka, K. Kuriyama, M. Yahagi, M. Satoh, K. Iwamura, C. Kim, Y. Kim, F. Shiraishi, K. Tsuji, and S. Minomura, Appl. Phys. Lett. **45**, 786 (1984).
[88]*The Physics of Hydrogenated Amorphous Silicon I,* edited by J. D. Joannopoulos and G. Lucovsky (Springer, Berlin, 1984).
[89]M. Taniguchi, M. Hirose, and Y. Osaka, J. Cryst. Growth **45**, 126 (1978).
[90]J. Magariño, D. Kaplan, A. Friederich, and A. Deneuville, Philos. Mag. B **45**, 285 (1982).
[91]B. S. Meyerson, B. A. Scott, and D. J. Wolford, J. Appl. Phys. **54**, 1461 (1983).
[92]Y. Ashida, Y. Mishima, M. Hirose, and Y. Osaka, J. Appl. Phys. **55**, 1426 (1984).
[93]M. Konagai, H. Takei, W. Y. Kim, and K. Takahashi, Proceedings of the 18th IEEE Photovoltaic Specialists Conference, Las Vegas, 1985 (unpublished).
[94]R. Bilenchi, I. Gianinoni, M. Musci, R. Murri, and S. Tacchetti, Appl. Phys. Lett. **42**, 279 (1985).
[95]C. C. Tsai, J. Knights, G. Chang, and B. Wacker, J. Appl. Phys. **59**, 2998 (1986).
[96]W. Paul, A. J. Lewis, G. A. N. Connell, and T. D. Moustakas, Solid State Commun. **20**, 969 (1976).
[97]D. Leidich, E. Linhart, E. Niemann, H. W. Grueninger, R. Fischer, and R. R. Zeyfang, J. Non-Cryst. Solids **59/60**, 613 (1983).
[98]J. H. Thomas, J. Vac. Sci. Technol. **17**, 1306 (1980).
[99]See, for example, A. J. Yarwood, O. P. Strausz, and H. E. Gunning, J. Chem. Phys. **41**, 1705 (1964).
[100]M. Stutzmann, R. J. Nemanich, and J. Stuke, Phys. Rev. B **30**, 3595 (1984).
[101]C. C. Tsai, M. Stutzmann, and W. B. Jackson, *Optical Effects in Amorphous Semiconductors,* AIP Conf. Proc. No. 120, edited by P. C. Taylor and S. G. Bishop, (AIP, New York, 1984), p. 242.
[102]L. J. Giling, Mat. Chem. Phys. **9**, 117 (1983).
[103]J. C. Knights, T. M. Hayes, and J. C. Mikkelsen, Jr., Phys. Rev. Lett. **39**, 712 (1977).
[104]M. Toulemonde, P. Siffert, A. Deneuville, and J. C. Bruyère, Appl. Phys. Lett. **39**, 152 (1981).
[105]J. A. Reimer and T. M. Duncan, Phys. Rev. B **27**, 4895 (1983).
[106]S. G. Greenbaum, W. E. Carlos, and P. C. Taylor, Solid State Commun. **43**, 663 (1982),
[107]S. G. Greenbaum, W. E. Carlos, and P. C. Taylor, J. Appl. Phys. **56**, 1874 (1984).
[108]J. I. Pankove, D. E. Carlson, J. E. Berkeyheiser, and R. O. Wance, Phys. Rev. Lett. **51**, 2224 (1983).
[109]N. M. Johnson, R. D. Burnham, R. A. Street, and R. L. Thornton, Phys. Rev. B **33**, 1102 (1986).
[110]N. M. Johnson, C. Herring, and D. J. Chadi, Phys. Rev. Lett. **56**, 769 (1986).
[111]R. A. Street, Phys. Rev. Lett. **49**, 1187 (1982).
[112]M. Stutzmann, Philos. Mag. B **53**, L15 (1986).
[113]R. A. Street, in *Proceedings of the 17th International Conference on the Physics of Semiconductors,* edited by D. J. Chadi and W. A. Harrison (Springer-Verlag, New York, 1985), p. 845.
[114]G. Müller, S. Kalbitzer, and H. Mannsperger, Appl. Phys. A **39**, 243 (1986).
[115]J. Robertson, J. Phys. C **17**, L349 (1984).
[116]J. Robertson, Phys. Rev. B **31**, 3817 (1985).
[117]J. C. Phillips, Phys. Rev. Lett. **42**, 1151 (1979).
[118]R. A. Street, D. K. Biegelsen, W. B. Jackson, N. M. Johnson, and M. Stutzmann, Philos. Mag. B **52**, 235 (1985).
[119]F. J. Kampas and P. E. Vanier, Phys. Rev. B **31**, 3654 (1985).
[120]D. Jousse (private communication).
[121]M. Stutzmann, in *Materials Issues in Amorphous Semiconductor Technology,* Mater. Res. Soc. Symp. Proc. No. 70, edited by D. Adler, Y. Hamakawa, and A. Madan (MRS, Pittsburgh, 1985), p. 203.
[122]W. Beyer and R. Fischer, Appl. Phys. Lett. **31**, 850 (1977).
[123]W. Beyer, R. Fischer, and H. Overhof, Philos. Mag. B **39**, 205 (1979).
[124]H. Overhof and W. Beyer, J. Non-Cryst. Solids **35/36**, 375 (1980).
[125]H. Pfleiderer, W. Kusian, and W. Krühler, Solid State Commun. **49**, 493 (1984).
[126]A. R. Hepburn, J. M. Marshall, C. Main, M. J. Powell, and C. van Berkel, Phys. Rev. Lett. **56**, 2215 (1986).
[127]M. Stutzmann, Philos. Mag. (to be published).